

Evolving turbulence and magnetic fields in galaxy clusters

Kandaswamy Subramanian,^{1,4*} Anvar Shukurov^{2,1,4} and Nils Erland L. Haugen^{3,5}

¹*Inter-University Centre for Astronomy and Astrophysics, Post Bag 4, Ganeshkhind, Pune 411 007, India*

²*School of Mathematics and Statistics, University of Newcastle, Newcastle upon Tyne, NE1 7RU, U.K.*

³*Department of Physics, Norwegian University of Science and Technology, Høyskoleringen 5, N-7034 Trondheim, Norway*

⁴*Isaac Newton Institute for Mathematical Sciences, 20 Clarkson Road, Cambridge, CB3 0EH, U.K.*

⁵*DAMTP, Centre for Mathematical Sciences, Wilberforce Road, Cambridge CB3 0WA, U.K.*

ABSTRACT

We discuss, using simple analytical models and MHD simulations, the origin and parameters of turbulence and magnetic fields in galaxy clusters. Any pre-existing tangled magnetic field must decay in a few hundred million years by generating gas motions even if the electric conductivity of the intracluster gas is high. We argue that turbulent motions can be maintained in the intracluster gas and its dynamo action can prevent such a decay and amplify a random seed magnetic field by a net factor typically 10^4 in 5 Gyr. Three physically distinct regimes can be identified in the evolution of turbulence and magnetic field in galaxy clusters. Firstly, the fluctuation dynamo will produce microgauss-strong, random magnetic fields during the epoch of cluster formation and major mergers. At this stage pervasive turbulent flows with r.m.s. velocity of about 300 km s^{-1} can be maintained at scales 100–200 kpc. The magnetic field is intermittent, has a smaller scale of 20–30 kpc and average strength of $2 \mu\text{G}$. Secondly, turbulence will decay after the end of the major merger epoch; we discuss the dynamics of the decaying turbulence and the behavior of magnetic field in it. Magnetic field and turbulent speed undergo a power-law decay, decreasing by a factor of two during this stage, whereas their scales increase by about the same factor. Thirdly, smaller-mass subclusters and cluster galaxies will produce turbulent wakes where magnetic fields will be generated as well. Although the wakes plausibly occupy only a small fraction of the cluster volume, we show that their area covering factor can be close to unity, and thus they can produce some of the signatures of turbulence along virtually all lines of sight. The latter could potentially allow one to reconcile the possibility of turbulence with ordered filamentary gas structures, as in the Perseus cluster. The turbulent speeds and magnetic fields in the wakes are estimated to be of order 300 km s^{-1} and $2 \mu\text{G}$, respectively, whereas the turbulent scales are of order 200 kpc for wakes behind subclusters of a mass $3 \times 10^{13} M_{\odot}$ and about 10 kpc in the galactic wakes. Magnetic field in the wakes is intermittent and has the scale of about 30 kpc and 1 kpc in the subcluster and galactic wakes, respectively. Random Faraday rotation measure is estimated to be typically $100\text{--}200 \text{ rad m}^{-2}$, in agreement with observations. We predict detectable polarization of synchrotron emission from cluster radio halos at wavelengths 3–6 cm, if observed at sufficiently high resolution.

Key words: galaxies: clusters: general – magnetic fields – MHD – turbulence

1 INTRODUCTION

Intergalactic gas in clusters of galaxies is magnetized (see reviews by Kronberg 1994; Carilli & Taylor 2002; Govoni & Feretti 2004). The number of clusters that exhibit detectable synchrotron emission is relatively small, but it is believed that a magnetic field is present in most clusters

(unlike relativistic electrons). Therefore, a more informative observational tracer of intracluster magnetic fields is Faraday rotation of the polarization plane of background radio sources and central radio galaxies. Clarke, Kronberg & Böhringer (2001) conclude, from their statistical study of Faraday rotation in 16 galaxy clusters, that random magnetic fields of a strength $(5\text{--}10) \times (l/10 \text{ kpc})^{-1/2} \mu\text{G}$ (with l the field scale) permeate the gas within about 500 kpc from the cluster centre; the area covering factor of magnetic fields is close to unity. The Faraday rotation measures detected

* E-mail: kandu@iucaa.ernet.in (KS); anvar.shukurov@ncl.ac.uk (AS); nils.haugen@phys.ntnu.no (NELH)

are about 200 rad m^{-2} for the lines of sight through clusters' central parts and about 100 rad m^{-2} farther out (see also Clarke 2004; Johnston-Hollitt & Ekers 2004). Important constraints on intracluster magnetic fields come from limits on X-ray emission produced from microwave background photons by inverse Compton scattering off relativistic electrons (Bagchi, Pislar & Lima Neto 1998; Sarazin 1988). Observational evidence is compatible with a random magnetic field of r.m.s. strength of $1\text{--}10 \mu\text{G}$ and coherence length of about $10\text{--}20 \text{ kpc}$.

Faraday rotation maps of a number of radio galaxies in clusters have also been analyzed. Eilek and Owen (2002) studied Faraday rotation maps of radio sources in the centres of the Abell clusters A400 and A2634, and found patches of RM fluctuations on scales about $10\text{--}20 \text{ kpc}$. Assuming this to be also the coherence scale for the field, these authors deduce field strengths of $1\text{--}4 \mu\text{G}$. Vogt and Enßlin (2003, 2005), using a novel technique (Enßlin & Vogt 2003), estimate magnetic field strength to be $3 \mu\text{G}$ in A2634, $6 \mu\text{G}$ in A400 and $7 \mu\text{G}$ in Hydra A. They obtain field correlation length of 4.9 kpc , 3.6 kpc and 3 kpc for these clusters, respectively. It cannot be excluded, however, that the Faraday rotation of cluster radio sources is contaminated by that arising in dense turbulent cocoons around the radio galaxies, rather than in the intracluster medium proper (Rudnick and Blundell 2003; see Enßlin et al. 2003 for another view). For this reason, the statistical studies of Faraday rotation of background radio sources, referred to above, provide perhaps a more convincing evidence for cluster-wide magnetic fields and their properties.

The origin of the cluster magnetic fields remains unclear. Carilli & Taylor (2002) (see also Tribble 1993a) argue that the small value of electric resistivity of the intracluster plasma guarantees that the decay time of magnetic field will be comparable to or exceed the cluster lifetime. They conclude that any magnetic field (e.g., that captured by a cluster during its formation) would survive for a long time. However, any inhomogeneous magnetic field will drive motions via the Lorentz force, and the motions will decay, plausibly in the form of decaying MHD turbulence (e.g., Biskamp 2003; see below). The turbulent decay time is comparable to the eddy turnover time of the largest eddies, about 10^8 yr , irrespective of the resistivity or viscosity of the gas. (Here we have taken a coherence scale of order 10 kpc for the field and the induced motions, with associated turbulent velocities of order 100 km s^{-1}). Although the energy density in MHD turbulence decays with time as a power law, this time scale is still much shorter than the typical age of a cluster, which is thought to be several billion years. Therefore, one has to provide explicit explanation of the origin and persistence of magnetic fields in the clusters; reference to the low Ohmic resistivity of the intracluster plasma is not sufficient if the gas is turbulent or the magnetic field is tangled.

An obvious option to explain intergalactic magnetic fields is to consider magnetic fields stripped from galaxies. Since the intracluster gas is enriched with metals, at least part of it originates in galaxies (Sarazin 1988). However, the strength of magnetic field produced by the stripping cannot exceed $\simeq 0.1 \mu\text{G}$ even in the cores of rich clusters and even if spiral galaxies with relatively strong large-scale field are involved (see Appendix A). Another possibility is that the intracluster field is supplied by active galaxies within the

cluster. As we discuss in Appendix A, this mechanisms can provide relatively strong magnetic field but fails to explain how the field can be maintained against turbulent decay. In addition, it is not quite clear how efficiently the magnetized relativistic plasma of the radio lobes can be mixed with the thermal intergalactic plasma and what would be the resulting scale of magnetic field. Altogether, the above mechanisms can only provide suitable seed magnetic field for the dynamo action in the intracluster plasma.

In most astrophysical systems, like disc galaxies, stars and planets, rotation is crucial for maintaining their magnetic fields, both by providing strong shear and by making (when coupled with stratification) random flows helical, and hence leading to mean-field dynamo action. However, galaxy clusters are believed to have fairly weak rotation (if any at all), so one has to appeal to some other mechanism for understanding cluster magnetism.

Another possibility to generate magnetic fields is related to the fluctuation dynamo action (Batchelor 1950; Kazantsev 1967), where random flow of electrically conducting fluid generates random magnetic field (Zeldovich, Ruzmaikin & Sokoloff 1990). This mechanism does not require any rotation or density stratification, and only relies on the random nature of the flow; so fluctuation dynamos can be active in virtually any turbulent environment where the plasma is ionized. Apart from the randomness of the flow, it is required that the magnetic Reynolds number is large enough, i.e., that the electric conductivity is high enough, and/or plasma motions are sufficiently intense, and/or their scale is sufficiently large.

The earliest theories of intracluster magnetic fields were based, implicitly or explicitly, on fluctuation dynamo theory under the assumption that galaxy clusters are steady-state turbulent systems (Jaffe 1980; Roland 1981; Ruzmaikin, Sokoloff & Shukurov 1989; Goldman & Rephaeli 1991; De Young 1992). The source of turbulence adopted by several authors were turbulent wakes of the cluster galaxies. This picture has to be reconsidered for several reasons.

Firstly, turbulence from galactic wakes can fill the cluster volume only if the effective galactic radius is of order 10 kpc (e.g., Ruzmaikin et al. 1989), i.e., if the interstellar gas is not stripped by the ram pressure of the intracluster gas. If the gas stripping is complete, the wake is only produced by gravitational accretion (Bondi 1952), and its radius is about the accretion radius $r_g = 2GM/(c_s^2 + V^2)$ where c_s is the speed of sound, V is the galactic speed, M is the galactic mass, and G is Newton's gravitational constant. For $c_s = 10^3 \text{ km s}^{-1}$, $V \approx c_s$ and $M = 10^{11} M_\odot$, the gravitational accretion radius $r_g \simeq 0.5 \text{ kpc}$ is much smaller than both the galactic radius and the apparent scale of the random magnetic field in the intergalactic gas (both usually assumed to be of order 10 kpc). Hence, sufficiently strong, volume-filling turbulent wakes whose width is comparable to the galactic size can only arise if the galaxies retain significant amounts of their interstellar gas. If the stripping of interstellar gas by ram pressure is efficient, galactic wakes are rather weak (Portnoy, Pistinner & Shaviv 1993; Balsara, Livio & O'Dea 1994; Acreman et al. 2003 and references therein; see however Toniazzo & Schindler 2001 who argue that the stripping efficiency is exaggerated in the above papers). Therefore turbulence generated in galactic wakes may not fill the cluster volume (see also Sect. 2.3.4).

Further, numerical simulations of De Young (1992), using a closure model, gave pessimistic estimates for magnetic fields produced by the dynamo when the turbulence is induced by galactic wakes. However, it is not clear if the resolution of those simulations (i.e., the effective magnetic Reynolds number) was high enough to obtain dynamo action, so this objection to the dynamo models is questionable. Recent direct simulations of dynamo action in turbulent flows (Haugen, Brandenburg & Dobler 2003, 2004; Schekochihin et al. 2004) have confirmed the efficiency of dynamo action in random non-helical flows.

Perhaps more importantly, cluster dynamics has been reconsidered recently, and the emerging picture is very different in that clusters may not be relaxed systems, but still remain in the state of formation via major mergers and accretion of smaller-mass subclusters. Numerical simulations and recent observations strongly suggest that a random flow, perhaps of turbulent nature, can be maintained for a few crossing times of the forming galaxy cluster (Norman & Bryan 1999). Roettiger et al. (1999a,b) have found that magnetic field can be amplified by these motions (see also results obtained with SPH simulations by Dolag, Bartelmann & Lesch 1999, 2002). However, the resolution of the simulations is still poor, and quantitative estimates of the turbulence parameters and especially of its effects on magnetic field are very uncertain.

In addition to the volume-filling flow produced during the cluster formation, significant random flows can still be generated in wakes behind infalling subclusters and cluster galaxies. These are not expected to fill the cluster volume, but we argue below that they can have significant area covering factor. There is also a possibility that radio galaxies can stir the intracluster gas as their plasma buoyantly rises through the gas (Brüggen et al. 2002; Enßlin & Heinz 2002). Another possible consequence of radio galaxy jets and/or lobes propagating at subrelativistic speeds through the cluster plasma, is the generation of turbulence in a cocoon surrounding the radio source (see for example Reynolds, Heinz & Begelman 2002).

The content of the paper is as follows. We consider the evolution of turbulence in the intracluster gas of a galaxy cluster during and after its formation in Sect. 2. Random flows produced during the merger epoch can lead to magnetic field generation via the fluctuation dynamo as discussed in Sect. 3. In Sects 2.2 and 4 we present evidence that the decay of both magnetic and kinetic energies after the epoch of major mergers will be a power law in time, rather than exponential, because of the turbulent nature of the flow. During the decay phase of the turbulence, the correlation scale of the magnetic field will grow (Frisch 1995; Olesen 1997; Biskamp & Müller 1999; Christensson, Hindmarsh & Brandenburg 2001), which slows down the decay of the Faraday rotation measure produced in the intracluster gas (Sect. 5.1). In Sect. 2.3 we argue that significant turbulence and magnetic field amplification can occur in turbulent wakes of smaller-mass subclusters and cluster galaxies. The turbulent wakes may not fill the volume, but can cover the cluster’s projected area (Sect. 2.3.2). We present order-of-magnitude estimates of the parameters of the random flows at various stages of the cluster evolution in Sect. 2, and of magnetic fields generated by the flows, in Sect. 3, which are further substantiated by numerical simulations of dy-

namo action in driven and decaying random flows discussed in Sect. 4. Faraday rotation measure and polarized radio emission produced by these magnetic fields are discussed in Sect. 5. Our results are summarized in Sect. 6 and Table 1.

2 INTRACLUSTER TURBULENCE

An upper limit on the turbulent velocity in a steady-state galaxy cluster follows from the requirement that the rate of dissipation of the turbulent energy should not exceed the X-ray luminosity of the cluster L_X , i.e., $\frac{1}{2}v_0^3/l_0 \lesssim L_X/M_g$, where v_0 and l_0 are the turbulent speed and scale, respectively, and M_g is the mass of the intergalactic gas. This yields

$$v_0 \lesssim 180 \frac{\text{km}}{\text{s}} \left(\frac{l_0}{200 \text{ kpc}} \right)^{\frac{1}{3}} \left(\frac{L_X}{10^{45} \text{ erg/s}} \right)^{\frac{1}{3}} \left(\frac{M_g}{10^{14} M_\odot} \right)^{\frac{1}{3}}. \quad (1)$$

This restriction applies to a steady state, and stronger turbulence can be driven in an evolving cluster, where the energy released by the decay of turbulent motions heats up the gas. Therefore, turbulent velocities significantly exceeding the above value can be considered as an indication of the cluster’s ongoing evolution. The turbulent nature of the flow is important, however: Eq. (1) only applies to turbulent flows and has to be reconsidered in the case of a random flow without turbulent energy cascade. As we argue below, turbulent motions during the epoch of cluster formation are intense enough to violate the constraint (1) because they keep evolving and their dissipation contributes to the heating of the intracluster gas to the virial temperature.

We now discuss various sources of turbulence in galaxy clusters.

2.1 Turbulence produced during cluster formation

Theories of hierarchical structure formation suggest that clusters of galaxies have been assembled relatively recently. N -body simulations indicate that the clusters form at the intersection of dark matter filaments in the large-scale structure, and result from both major mergers of objects of comparable mass (of order $10^{15} M_\odot$) and the accretion of smaller clumps onto massive protoclusters. It is likely that intense random vortical flows, if not turbulence, are produced in the merger events (Kulsrud et al. 1997; Norman & Bryan 1999; Ricker & Sarazin 2001). These would originate not only due to vorticity generation in oblique accretion shocks and instabilities during the cluster formation, but also in the wakes of the smaller clumps. In this section we summarize some of the work on the cluster-wide turbulence resulting from major mergers. Its consequences for the generation of cluster magnetic fields are considered in Sect. 3.

There have been several numerical simulations of gas dynamics during the formation of galaxy clusters. Norman & Bryan (1999) find that the intracluster medium becomes turbulent during cluster formation, with turbulent velocities of about 400 km s^{-1} within 1 Mpc from the centre of a cluster and eddy sizes ranging from 50 to 500 kpc; the random flow is volume filling (see also Sunyaev, Norman & Bryan 2003). In the cluster merger model of Ricker & Sarazin (2001), ram pressure displaces gas in the cluster core from the bottom of

the potential well. The resulting convective plumes produce large-scale disordered motions with eddy size up to several hundred kiloparsecs; even after 15 Gyr of evolution, turbulent velocities in the inner parts remain at a surprisingly high level of 10–40% of the sound speed (i.e., 100–400 km s⁻¹), and grow up to the sound speed in the outer parts.

Observational evidence of intracluster turbulence is scarce. From analysis of pressure fluctuations as revealed in X-ray observations, Schueker et al. (2004) argue that the integral turbulent scale in the Coma cluster is close to 100 kpc, and they assume a turbulent speed of 250 km s⁻¹ at that scale. The nonthermal broadening, by the turbulence, of X-ray spectral lines of ionized iron can be detectable with future X-ray observatories (Inogamov & Sunyaev 2003).

The spatial resolution of all available simulations is rather coarse (of order 10 kpc or worse) and only comparable with the apparent scale of the intracluster magnetic field. Even if the random nature of the resulting flow is obvious, it is not clear if it will evolve into developed turbulence, i.e., if the turbulent cascade is established to carry energy to small scales where it dissipates into heat. From the viewpoint of magnetic field generation, the presence of turbulence as such is not required; the randomness of the flow is sufficient (Kazantsev 1967; Zeldovich et al. 1990). However, the dynamics of the flow and its evolution do depend on whether or not the turbulent cascade persists (see Sect. 2.2).

The flow can become turbulent if the kinematic Reynolds number in the intracluster gas, Re , is large enough. Following Sarazin (1988) and Ricker & Sarazin (2001), an estimate of Re can be obtained as

$$Re = \frac{v_0 l_0}{\nu} \simeq 3 \frac{v_0 l_0}{c_s \lambda \delta} = 3\mathcal{M} \frac{l_0}{\lambda \delta}, \quad (2)$$

where $\nu = \frac{1}{3} c_s \lambda \delta$ is the effective kinematic viscosity, c_s is the speed of sound (assumed to be close to the thermal speed), \mathcal{M} is the Mach number, λ is the ion mean free path, and subscript ‘0’ refers to the energy-range values. Here we have introduced parameter δ that quantifies the poorly understood behaviour of viscosity in the intracluster plasma. The standard, Spitzer’s value of λ can be written as

$$\lambda \simeq 5 \text{ kpc} \left(\frac{c_s}{10^3 \text{ km s}^{-1}} \right)^4 \left(\frac{n_e}{10^{-3} \text{ cm}^{-3}} \right)^{-1},$$

with n_e the electron number density. For $\mathcal{M} \simeq 1$, $l_0 \simeq 100$ –500 kpc and $\lambda \gtrsim 1$ kpc, this yields $Re \lesssim (300\text{--}1500)\delta^{-1}$. This estimate is, however, suspect because the mean free path is comparable to the scale of inhomogeneities in the gas. It is also clear that even a weak seed intracluster magnetic field could strongly reduce the effective viscosity and make it anisotropic. The effective Reynolds number can be significantly larger if any shorter length scale plays the role rather than the Coulomb mean free path, or a frequency higher than the ion collision frequency (these may be associated with plasma instabilities and/or waves). Schekochihin et al. (2005b) argue that the firehose and/or mirror instabilities can provide the effective diffusion in the magnetized plasma; the corresponding length scale is the ion gyroradius, a quantity normally much smaller than the mean free path. These uncertainties are allowed for, in a heuristic manner, by choosing $\delta < 1$; Fabian et al. (2005) scale their results by $\delta = 0.1$. This prescription can be an oversimplification as it omits plausibly important physical effects arising from the

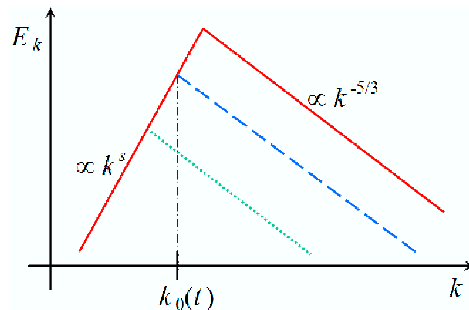


Figure 1. The evolution of the spectrum of decaying turbulence, where the spectral exponent remain constant both in the inertial range, where it is equal to s , and at large scales where it is equal to $-5/3$. Solid, dashed and dotted lines show the spectrum at consecutive times. As the energy dissipates, the energy-range wave number k_0 reduces.

anisotropy of viscosity in magnetized plasma (cf. Schekochihin et al. 2005b). However, even if one cannot readily provide a confident estimate of Re , Eq. (2) suggests that it will be large enough as to ensure that random motions driven by major merger events can become turbulent. Only this fact is important for our purposes in this paper. Our simulations of a flow driven by external random force (Sect. 4) have been performed for $Re = 100$ –400, and they do indeed show a flow with broad range of scales typical of turbulent flows (and so inertia forces dominate over viscosity), even if the inertial range is not wide at these modest Reynolds numbers.

To summarize, the above results seem to converge to the following picture. Random motions driven in major merger events have the typical initial speed of $v_{0i} \simeq 300$ km s⁻¹ and scale $l_{0i} \simeq 100$ –200 kpc, so that the turnover time of the energy-range eddy is $t_{0i} = 0.3$ –0.6 Gyr. The random motions will be maintained at this level during the major merger epoch, whose duration can be as large as $t_f \simeq 3$ –5 Gyr. (The notation is motivated in Sect. 2.2.)

2.2 Dynamics of decaying turbulence

The random flows produced by major mergers will not remain statistically steady after the end of the merger event. Unlike a laminar flow that decays exponentially in time due to viscosity, turbulent kinetic energy decays slower, as a power law (e.g., Landau & Lifshitz 1975, Frisch 1995). The reason for this is that kinetic energy mainly decays at small scales, to where it is constantly supplied by the turbulent cascade. As a result, the energy decay rate depends nonlinearly on the energy itself, which makes the decay a power law in time. (The corresponding calculation is provided below.) Our simulations of Sect. 4 confirm that the power-law decay occurs even for the Reynolds number as small as $Re \approx 100$.

In this section we review simple models of decaying hydrodynamic turbulence. The effects of magnetic field on the flow can be neglected at early stages when magnetic field is still weak. In Sect. 4 we present numerical simulations where the effects of magnetic field on the flow are fully allowed for.

Consider an initial spectrum of turbulence shown with solid line in Fig. 1, where $E_k = Ck^s$ (with $s > -1$) at scales $k < k_0$, and $E_k \propto k^{-5/3}$ at smaller scales as in Kolmogorov turbulence. Here kE_k is the specific energy per unit loga-

rhythmic interval in the k -space. It is related to the turbulent velocity at wave number k via $v_k \propto (kE_k)^{1/2}$; E_k has a maximum at a certain wave number k_0 , which is therefore called the energy-range wave number. Turbulent flow remains in a statistically steady state despite viscous dissipation at small scales if it is driven at larger scales. When such a driving ceases, the turbulence decays.

Motions at small scales are the first to be affected by viscosity. It is reasonable to expect that the exponent s and constant C are preserved during the decay (e.g., Sect. 7.7 of Frisch 1995). Consider the time-dependent total specific turbulent energy $E(t)$, which is approximately equal to that at the energy-range scale, $E(t) \simeq \frac{1}{2}v_0^2$, if the inertial part of the spectrum is steep enough. On the other hand, $E(t) = \int_0^\infty E_k dk \propto k_0^{s+1}$. As long as the Reynolds number remains large, and so viscosity at k_0 is negligible, energy at the energy-range wave number $k_0(t)$ mainly decays because it cascades to smaller scales. Hence, the energy loss rate is given by $dE/dt = -v_0^2/t_0 \simeq -v_0^3 k_0$, where $t_0 \simeq (v_0 k_0)^{-1}$. Since $v_0 \propto E^{1/2}$ and $k_0 \propto E^{1/(s+1)}$, the evolution of the total turbulent energy is governed by

$$\frac{dE}{dt} \simeq -AE^{(3s+5)/[2(s+1)]}, \quad (3)$$

where A is a certain constant related to C . This equation can easily be integrated (for constant C) to yield (see Fig. 1) asymptotic forms (applicable at large t) for the energy decay law

$$E(t) \propto t^{-\alpha},$$

and for the energy-range scale growth law

$$l_0 \propto k_0^{-1} \propto t^\beta,$$

where

$$\alpha = 2\frac{s+1}{s+3}, \quad \beta = \frac{2}{s+3}.$$

The value $s = 2$ gives a ‘white noise’ spectrum at large scales, where the three-dimensional spectrum $k^{-2}E_k$ is flat. In this case

$$\alpha = 6/5, \quad \beta = 2/5.$$

Another possibility often considered in this context is $s = 4$, where one gets $\alpha = 10/7$ and $\beta = 2/7$ (Skrbek & Stalp 2000; Touil, Bertoglio & Shao 2002).

There are arguments suggesting that $s = 2$ is a better acceptable value than $s = 4$; in particular, the coefficient C is time-dependent for $s = 4$, and this makes the energy decay significantly slower than that obtained above (Frisch 1995). Also $s = 4$ would be relevant for an incompressible flow, whereas the cluster flows are expected to be mildly compressible, and $s = 2$ could be more appropriate. The turbulence decay is sensitive to the detailed physical nature of the system, and it is often slower than derived above. The decay of the MHD turbulence can be significantly slowed down if the system has non-zero invariants such as magnetic helicity and/or cross-helicity (Biskamp 2003). If the intracluster seed magnetic fields are due to stripping of the galactic magnetic fields, then they may have both types of helicities. The decay law is also sensitive to the relation between the turbulent energy-range scale and the size of the system; the decay speeds up to become $E \propto t^{-2}$ when the two scales become

comparable and the value of k_0 cannot decrease any further (Skrbek & Stalp 2000; Touil et al. 2002).

We adopt $\alpha = 6/5$ and $\beta = 2/5$ for numerical estimates in what follows, so that

$$E \simeq \frac{1}{2}v_0^2 \propto \left(\frac{t-t_f}{t_{0i}}\right)^{-6/5}, \quad k_0 \propto \left(\frac{t-t_f}{t_{0i}}\right)^{-2/5}, \quad (4)$$

for $t - t_f \gg t_{0i}$, where subscript ‘i’ refers to the start of the evolution, t_{0i} is a certain dynamical time scale, which can be identified with the initial turnover time of the energy-containing eddies, $t_{0i} = l_{0i}/v_{0i}$, subscript ‘0’ refers to the energy-range (correlation) scale of the motion (which varies with time), and the decay starts at time $t = t_f$ when the flow forcing ceases. This decay is faster than in many other models of decaying turbulence; thus, our conclusions will be rather conservative with respect to the intensity of turbulence at late times.

With the above decay law of turbulence, the Reynolds number evolves slowly as

$$\text{Re} \propto \left(\frac{t-t_f}{t_{0i}}\right)^{-1/5}, \quad t - t_f \gg t_{0i}.$$

Allowing for the initial period $t_f = 3$ Gyr of sustained turbulence, Re decreases only by a factor of 1.4 after the total evolution time of $t = 6$ Gyr for $l_{0i} = 150$ kpc and $v_{0i} = 300$ km s $^{-1}$ (yielding $t_{0i} = 0.5$ Gyr).

2.3 Minor mergers and turbulent wakes

Consider the infall of relatively small subclusters of mass m into an already formed cluster of mass M . Define $d^2p/(d(\ln m) dt)$ as the probability that in a time dt a subcluster, whose mass belongs to a logarithmic mass interval $[\ln m, \ln m + d(\ln m)]$, merges with the bigger cluster of mass M . The merger rate $d^2p/(d(\ln m)dt)$ scales with the subcluster mass as (Lacey & Cole 1993)

$$\frac{d^2p}{d(\ln m) dt} \propto m^{-1/2} \quad \text{for } \frac{m}{M} \ll 1. \quad (5)$$

Thus, the merger rate of masses of order $10^{13}M_\odot$ is about 10 times larger than that for $10^{15}M_\odot$. If major mergers of masses of order $10^{15}M_\odot$ occur once in 3 Gyr, the time interval between mergers with $10^{13}M_\odot$ subclusters will then be of the order of 0.3 Gyr (see also Norman & Bryan 1999). Such minor mergers are thought to play an important role in explaining the observed cold fronts in clusters (Heinz et al. 2003; Motl et al. 2004 and references therein). They can also generate turbulence in the wake of a moving subcluster (cf. recent simulations of Takizawa 2005). Turbulence generated by subclusters was suggested by Norman and Bryan (1999) to be a major source of the random motions observed in their simulations of cluster formation. Here we examine this issue further with analytical estimates, using parameters of galaxy clusters and smaller structures obtained from hierarchical theories of structure formation.

2.3.1 Ram pressure stripping

The subclusters contain gas which can be partially stripped by hydrodynamic interaction with the cluster gas (by ram pressure stripping and via hydrodynamic instabilities)

(Fabian & Daines 1991; Acreman et al. 2003). A simple criterion for the radius R_0 within which the subcluster gas remains unstripped can be obtained as follows. The ram pressure force exerted on a gas sphere of radius R_0 is equal to $\rho_c v_{sc}^2 \pi R_0^2$, where ρ_c is the intracluster gas density and v_{sc} is the speed at which the subcluster moves through the intracluster gas. Following Fabian & Daines (1991), we note that the gravitational restoring force per unit area due to the subcluster mass is comparable to the gas pressure in the subcluster, assuming that the subcluster is in hydrostatic equilibrium. The gas sphere will be removed from the subcluster if the restoring force is smaller than the ram pressure force. Thus, a local criterion for retaining the gas at a distance R_0 from the subcluster centre is

$$\rho_c v_{sc}^2 \leq f \rho_{sc}(R_0) u^2, \quad (6)$$

where $\rho_{sc}(R)$ is the gas density distribution of the subcluster, R is the subcluster's spherical radius, f is a numerical factor of order unity, and u is the gas velocity dispersion within the subcluster. We adopt, for illustrative purposes, gas density profiles for the cluster and subcluster, respectively, of the form

$$\rho_c(r) = \frac{\rho_{c0}}{[1 + (r/r_c)^2]}, \quad \rho_{sc}(R) = \frac{\rho_{sc0}}{[1 + (R/R_{sc})^2]},$$

where ρ_{c0} and ρ_{sc0} are the respective central gas densities and r_c and R_{sc} are the corresponding gas core radii. (These correspond to the standard β -profile with the slope parameter $\beta = 2/3$ – Sarazin 1988). From Eq. (6), the subcluster gas is retained at radii smaller than R_0 , where

$$\left(\frac{R_0}{R_{sc}}\right)^2 = f \frac{\rho_{sc0} u^2}{\rho_{c0} v_{sc}^2} \left[1 + \left(\frac{r}{r_c}\right)^2\right] - 1. \quad (7)$$

Takeda, Nulsen & Fabian (1984) suggest $f \simeq 2$.

Parameters of clusters and subclusters that enter Eq. (7) vary broadly in both observed and simulated clusters. Suitable values can be selected as follows. For example, consider subclusters predicted by the hierarchical theory of structure formation (Peebles 1980; Padmanabhan & Subramanian 1992; Padmanabhan 1993). Suppose that the initial density fluctuations can be described as a Gaussian random field with the r.m.s. density contrast $\sigma_m(m)$, where m is the mass of the structure. In the hierarchical theory, $\sigma_m(m) \propto m^{-(3+n)/3}$ with n close to -1 at the cluster scales and to -2 at the galactic scales. For a density fluctuation which is μ times the above r.m.s. value, the following scaling laws can be obtained: $r_{vir} \propto \mu^{-1} m^{(n+5)/6}$ for the virial radius; $u^2 \simeq Gm/r_{vir} \simeq \mu m^{(1-n)/6}$ for the virial velocity; and $\rho \propto m/r_{vir}^3 \propto \mu^3 m^{-(n+3)/2}$ for the average gas density. This suggests the average pressure scaling

$$\rho_{sc} u^2 \propto \mu^4 m^{-2(n+2)/3}.$$

We adopt $n = -1.5$, $M = 10^{15} M_\odot$, $m = 3 \times 10^{13} M_\odot$, and a bulk velocity of the subcluster of order the cluster velocity dispersion, $v_{sc} \simeq 1000 \text{ km s}^{-1}$. For comparison, the merging components of the Coma cluster have virial masses $0.9 \times 10^{15} M_\odot$ and $6 \times 10^{13} M_\odot$ (Colless & Dunn 1996). We also assume that the cluster and subcluster correspond to density fluctuations of the same value of μ . Then Eq. (7) yields $R_0 = 2.3 R_{sc}$ at the cluster centre, $r = 0$, and $R_0 = 3.4 R_{sc}$ at the cluster core radius, $r = r_c$. So, according to this criterion, gas within 2–3 subcluster core radii will not

be stripped as the subcluster falls, along a radial orbit, into a cluster which is about 30 times larger in mass.

Further, we take the gas core radius to be proportional to the virial radius. Indeed, Sanderson and Ponman (2003) suggest that the gas core radius is about $0.1 r_{vir}$ for clusters with temperature exceeding 1 keV, or the mass of a few times $10^{13} M_\odot$. Then the subcluster gas core radius is about $(m/M)^{(n+5)/6} \approx 0.13$ times the cluster gas core radius for $m/M = 0.03$. For a rich cluster with the virial radius 3 Mpc and the core radius ten times smaller, or $r_c = 300 \text{ kpc}$, we obtain the subcluster gas core radius as $R_{sc} \simeq 40 \text{ kpc}$. This implies for such subclusters the stripping radius of at least

$$R_0 \simeq 100 \text{ kpc}.$$

We adopt these values for qualitative estimates, keeping in mind that scatter about the fiducial values is likely to be large.

Heinz et al. (2003) simulated a subcluster with a shallower gas density profile ($\beta = 0.5$), a somewhat large core radius $R_{sc} = 250 \text{ kpc}$, central gas number density $\rho_{sc0} = 3.6 \times 10^{-3} \text{ cm}^{-3}$ and a temperature $T = 3.2 \text{ keV}$, moving through a uniform gas of a density $\rho_{c0} = 4.6 \times 10^{-4} \text{ cm}^{-3}$ and temperature $T = 7.7 \text{ keV}$. These authors find that the subcluster gas within $R_0 \simeq 2 R_{sc}$ survives ram pressure stripping, which compares favourably with our estimates based on Eq. (6).

Flow past a solid sphere develops into a turbulent wake for sufficiently large Reynolds numbers. Experiments and numerical simulations (Tomboulides & Orszag 2000 and references therein) show that the transition to turbulence occurs at $Re \approx 400$, via the Kelvin–Helmholtz instability of a shear layer that results from the separation of the boundary layer on the sphere's surface. It is not clear what is the critical Reynolds number for a gaseous sphere. It can be speculated that the entrainment of the dense subcluster gas into the flow can be a cause of the flow randomness additional to that past a solid sphere. The Kelvin–Helmholtz instability does indeed develop on the boundary between the subcluster and the ambient gas, e.g., in the simulations of Takizawa (2005) among many other authors, leading to prominent eddy-like structures in the subcluster wake that can be described as a turbulent flow.

Nulsen (1982) describes how the introduction of eddies of a scale l can make the boundary layer smooth on this scale, suppressing the Kelvin–Helmholtz instability at wavelengths smaller than l . Longer-wavelength modes are still unstable, and the largest unstable scales are comparable to the stripping radius. The Kelvin–Helmholtz instability is efficient in eventually removing gas from the subcluster. According to Heinz et al. (2003), all the gas is removed after a time of order a few times $10 R_0 / v_c$, that is a few billion years. This implies that a subcluster can generate a turbulent wake during one or two passages through the cluster.

Altogether, the flow produced by the Kelvin–Helmholtz instability can produce turbulence in the subcluster's wake, subject to the same reservations as discussed after Eq. (2). It is then plausible that the wake far downstream of the subcluster is well described by Prandtl's self-similar solution for turbulent wakes.

2.3.2 The area covering and volume filling factors of turbulent wakes

Prandtl's solution for the turbulent scale and velocity variation with distance x along the wake has the form (Landau & Lifshitz 1975)

$$l_{0x} \simeq L_i(x/L_i)^{1/3}, \quad v_{0x} \simeq V_i(x/L_i)^{-2/3}, \quad (8)$$

where the turbulent velocity near the head of the wake can be identified with some fraction of the subcluster speed, $V_i \simeq v_c \simeq 1000 \text{ km s}^{-1}$; and the initial value of the turbulent scale L_i is close to the stripping radius R_0 estimated above, $L_i \simeq R_0$. The Reynolds number varies along the wake as

$$\text{Re}(x) = \text{Re}_i(x/R_0)^{-1/3}, \quad \text{Re}_i = \frac{L_i V_i}{\nu},$$

and we assume that the wake remains turbulent as long as the Reynolds number exceeds a certain critical value, Re_{cr} . Then the length of a turbulent wake, X , follows from $\text{Re}(X) = \text{Re}_{\text{cr}}$ as

$$\frac{X}{R_0} \simeq \left(\frac{\text{Re}_i}{\text{Re}_{\text{cr}}} \right)^3, \quad (9)$$

where $\text{Re}_{\text{cr}} = 400$ (Tomboulides & Orszag 2000) can be adopted for illustrative purposes. Thus, we assume that the critical value of Re required to maintain turbulence within the wake is the same as that to produce it immediately behind a solid sphere. This will result in a quite conservative estimate of the wake length since turbulence can plausibly sustain at even smaller local values of Re .

The area of a single wake of a length X seen from the side is given by

$$S = 2 \int_{R_0}^X R_0(x/R_0)^{1/3} dx = \frac{3}{2} R_0^2 \left[\left(\frac{X}{R_0} \right)^{4/3} - 1 \right].$$

If the wake axis is inclined by a random angle α to the line of sight, where α is uniformly distributed with $0 \leq \alpha \leq \pi$, the average area of a single wake in the sky plane is given by

$$\bar{S} = \xi S, \quad \xi = \frac{1}{2} \int_0^\pi \sin^{7/3} \alpha d\alpha \approx 0.74.$$

The area covering factor of N wakes within a region larger in diameter $2r$ than the wake length, $r > X/2$, follows as

$$f_S = \frac{N \bar{S}}{\pi r^2} \simeq \frac{3}{2\pi} N \xi \left(\frac{R_0}{r} \right)^2 \left[\left(\frac{X}{R_0} \right)^{4/3} - 1 \right]. \quad (10)$$

Similarly, the volume filling factor of N wakes is given by

$$f_V \simeq \frac{9}{20} N \left(\frac{R_0}{r} \right)^3 \left[\left(\frac{X}{R_0} \right)^{5/3} - 1 \right]. \quad (11)$$

Both estimates assume that the wakes do not intersect in three dimensions, which makes them slight overestimates.

The r.m.s. turbulent velocity averaged over the wake length X is given by

$$\begin{aligned} v_0 &= \left(X^{-1} \int_0^X v_{0x}^2 dx \right)^{1/2} \\ &\simeq \sqrt{3} V_i \left\{ \frac{R_0}{X} \left[1 - \left(\frac{R_0}{X} \right)^{1/3} \right] \right\}^{1/2} \end{aligned}$$

$$\simeq \sqrt{3} V_i \left(\frac{\text{Re}_{\text{cr}}}{\text{Re}_i} \right)^{3/2} \left(1 - \frac{\text{Re}_{\text{cr}}}{\text{Re}_i} \right)^{1/2}. \quad (12)$$

Similarly, the typical turbulent scale can be identified with the average wake width,

$$l_0 \simeq \frac{3}{4} R_0 (X/R_0)^{1/3}. \quad (13)$$

The area covering factor and the volume filling factor of the wakes sensitively depend on the subcluster mass m and are larger for larger m (which is consistent with the idea that turbulence produced in major merger events fills the volume). We also note the strong dependence of the covering and filling factors on the Reynolds number: $f_S \propto \text{Re}^4$ and $f_V \propto \text{Re}^5$ (for $X/R_0 \gg 1$).

It is clear from Eqs (10) and (11) that one can have $f_V \ll 1$ but $f_S \simeq 1$ (note that $R_0 \ll r$). When this is the case, the wakes are widely separated in space, but their images overlap in the two-dimensional projection onto the sky plane.

2.3.3 Subcluster wakes

For subclusters of a mass $m = 3 \times 10^{13} M_\odot$, we adopt $R_0 = 100 \text{ kpc}$, $V_i = c_s$ and $\lambda = 1 \text{ kpc}$ to obtain, from Eq. (9), an estimate

$$\frac{X}{R_0} \simeq 27 \left(\frac{R_0}{100 \text{ kpc}} \right)^3 \left(\frac{4\lambda\delta}{1 \text{ kpc}} \right)^{-3} \left(\frac{\text{Re}_{\text{cr}}}{400} \right)^{-3}. \quad (14)$$

With the scaling of Eq. (5), the merger rate of subclusters of this mass is about 5 times larger than that of major mergers; thus, we assume that $N = 5$ subclusters of this mass can (almost) simultaneously fall into a larger cluster. The area covering and volume filling factors of $N = 5$ wakes within the radius $r = r_{\text{vir}} \approx 3 \text{ Mpc}$ are estimated as

$$f_S \simeq 0.2 \xi \frac{N}{5} \left(\frac{R_0}{100 \text{ kpc}} \right)^6 \left(\frac{\text{Re}_{\text{cr}}}{400} \right)^{-4} \left(\frac{4\delta\lambda}{1 \text{ kpc}} \right)^{-4},$$

and

$$f_V \simeq 0.02 \frac{N}{5} \left(\frac{R_0}{100 \text{ kpc}} \right)^8 \left(\frac{\text{Re}_{\text{cr}}}{400} \right)^{-5} \left(\frac{4\delta\lambda}{1 \text{ kpc}} \right)^{-5}.$$

The covering and filling factors strongly depend on the poorly known viscosity, parameterized with δ . For $\delta \lesssim 0.16$, we obtain $f_S \gtrsim 1$, but the volume filling factor remains smaller than unity for $\delta \gtrsim 0.1$. Furthermore, both f_S and f_V depend on high powers of another poorly known parameter, the stripping radius R_0 . Hence, properties of the subcluster wakes can be rather different in apparently similar clusters. In addition, results of numerical simulations of turbulent wakes should be treated with caution as otherwise reasonable approximations, numerical resolution, and numerical viscosities can strongly affect the results.

Upper limits on the covering and filling factors follow if we assume that the wake length is equal to or exceeds the region size, $X = 2r_{\text{vir}} = 6 \text{ Mpc}$, which is obtained in Eq. (9) if $\text{Re}_i/\text{Re}_{\text{cr}} > 4$ (and $\lambda = 1 \text{ kpc}$):

$$f_S \lesssim 0.5(4\delta)^{-4}, \quad f_V \lesssim 0.08(4\delta)^{-5},$$

which yields $f_S \lesssim 2$ and $f_V \lesssim 0.5$ for $\delta \gtrsim 0.2$.

Thus, wakes from subclusters of a mass $3 \times 10^{13} M_\odot$ can occupy just a small fraction of the total volume within the

viral radius of a cluster, but their area covering factor can be substantial. Given the sensitive dependence on the poorly known value of the Reynolds number, it appears reasonable to assume that $f_S = O(1)$, that is any line of sight within the virial radius will have good chance to intersect at least one turbulent wake.

The r.m.s. turbulent velocity averaged over the wake length follows from Eq. (12) as $v_0 \simeq 260 \text{ km s}^{-1}$ if averaged along the whole length $X \simeq 2.7 \text{ Mpc}$, and $v_0 \simeq 190 \text{ km s}^{-1}$ within the cluster virial radius (with $X = 2r_{\text{vir}} \simeq 6 \text{ Mpc}$). The average turbulent scale follows from Eq. (13) as $l_0 \simeq 200 \text{ kpc}$.

Takizawa (2005) has recently studied turbulence generated by a subcluster of total mass of $10^{14} M_\odot$, gas core radius of 100 kpc and a much higher central density $\simeq 3 \times 10^{-2} \text{ cm}^{-3}$, moving through a uniform medium about 100 times less dense. Turbulent velocities obtained in those simulations, 300–500 km s^{-1} (see also Norman & Bryan 1999; Ricker & Sarazin 2001; Schueker et al. 2004), are in a reasonable agreement with our estimates.

2.3.4 Galactic wakes

The stripping radius of galaxies could be estimated similarly to that of subclusters, but the arguments are complicated by the replenishment of interstellar gas by stellar winds, magnetic fields that affect the Kelvin–Helmholtz instability, etc. Both numerical models (Portnoy et al. 1993; Balsara et al. 1994; Acreman et al. 2003) and observations (Sun et al. 2005) indicate that gas within

$$R_0 = 3\text{--}5 \text{ kpc} \quad (15)$$

of the centre of a massive elliptical galaxy can remain unstripped. We assume that the Reynolds number based on this scale, $\text{Re} \simeq (10\text{--}15)\delta^{-1}$, is large enough to produce a turbulent wake, e.g., because δ is small enough.

Consider a rich galaxy cluster, where $N \approx 100$ galaxies are found within the gas core radius $r_c = 180 \text{ kpc}$ (Sarazin 1988). From Eq. (10), the area covering factor of galactic wakes in this region is unity if

$$\frac{X}{R_0} \simeq 30\text{--}15, \quad X \simeq 100\text{--}70 \text{ kpc}, \quad (16)$$

where the range corresponds to that in Eq. (15). Wakes of this length would require $\text{Re}_i/\text{Re}_{\text{cr}} \simeq 3$, which is obtained, e.g., for $\delta \simeq 0.01$ if $\text{Re}_{\text{cr}} = 400$.

The r.m.s. turbulent velocity and scale averaged along the wake follow from Eqs (12) and (16) as

$$v_0 \simeq 300 \text{ km s}^{-1}, \quad l_0 \simeq 8 \text{ kpc} \quad (17)$$

for $R_0 = 4 \text{ kpc}$ and $X/R_0 = 20$. The volume filling factor of such wakes is $f_V \simeq 0.07$.

The size of galactic wakes required to cover the projected cluster area, given by Eq. (16), does not seem to be unrealistic. For example, Sakelliou et al. (2005) have observed a wake behind a massive elliptic galaxy (mass of order $2 \times 10^{12} M_\odot$) moving through the intracluster gas at a speed about $v_c \simeq 1000 \text{ km s}^{-1}$. The length of the detectable wake is about $X \simeq 130 \text{ kpc}$ (assuming that it lies in the sky plane), and its mean radius is 40 kpc (obtained from the quoted volume of about $2 \times 10^6 \text{ kpc}^3$). These authors argue that the wake is produced by the ram pressure stripping of

the interstellar gas. The projected area of the wake is about 10^4 kpc^2 , as compared to 10^3 kpc^2 for the wake parameters derived above. This wake has been detected only because it is exceptionally strong, and it is not implausible that weaker but more numerous galactic wakes can cover the area of the central parts of galaxy clusters.

We conclude that subcluster wakes are likely to be turbulent, but galactic wakes can be laminar if the viscosity of the intracluster gas is as large as Spitzer’s value. Given the uncertainty of the physical nature (and hence, estimates) of the viscosity of the magnetized intracluster plasma, we suggest that turbulent galactic wakes remain a viable possibility. Both types of wake have low volume filling factor but can have an area covering factor of order unity.

3 MAGNETIC FIELD IN THE INTRACLUSTER GAS

In this section we discuss the amplification of an initially weak seed magnetic field by the fluctuation dynamo operating in the intracluster gas. The seed field itself can be produced by a wide range of mechanisms (Appendix A; see also Ruzmaikin et al. 1989; Widrow 2002; Brandenburg & Subramanian 2005). We first discuss the fluctuation dynamo in general terms. These general ideas are then applied to the various contexts of intracluster turbulence discussed above. First, we consider the merger epoch when the turbulence can be assumed to be in a statistically steady state, then the later epochs after the driving by the merger had ceased and the turbulence decays, and finally to magnetic field generation in turbulent wakes.

3.1 The fluctuation dynamo

The evolution of a magnetic field embedded into a flow of conducting fluid is controlled by the magnetic Reynolds number defined, similarly to Eq. (2), as

$$R_m = \frac{v_0 l_0}{\eta},$$

where η is the magnetic diffusivity (inversely proportional to the electric conductivity).

The exponentially fast amplification of an initially weak magnetic field by a random flow (called the *fluctuation dynamo*) is a result of a random stretching of magnetic field by the local velocity shear (see reviews in Zeldovich et al. 1990 and Brandenburg & Subramanian 2005). For $R_m \gg 1$, magnetic field is nearly frozen into the flow. Then, due to the random stretching, magnetic field lines grow longer, that is B/ρ increases, where ρ is the gas density. For flows with ρ approximately constant, the magnetic field will be amplified. Such amplification comes at the cost of a decrease in the scale of field structures in the directions perpendicular to the stretching (i.e., on average in all directions if the flow is statistically isotropic). This enhances Ohmic dissipation and the latter ensures that the correlation function of magnetic field can grow exponentially as an eigenfunction if the Lorentz force is negligible (the kinematic dynamo). The growth occurs under a fairly weak condition $R_m > R_{m,\text{cr}} \simeq 30\text{--}100$ (where the variation within the range depends on the form of the velocity correlation function). If

v_l is the velocity at a scale l , the e -folding time for the magnetic field is roughly equal to the eddy turnover time l/v_l . In the Kolmogorov turbulence, where $v_l \propto l^{1/3}$, the e -folding time is shorter at smaller scales, $l/v_l \propto l^{2/3}$, and so smaller eddies amplify the field faster.

Since $\eta \ll \nu$ in the rarefied intracluster plasma (e.g., Brandenburg & Subramanian 2005), we have $R_m \gg \text{Re}$. Therefore, $R_m \gg R_{m,\text{cr}}$ if $\text{Re} \gtrsim 100$, so that random motions in galaxy clusters will be a dynamo for any Reynolds number which is large enough to make them turbulent.

Numerical simulations of magnetic field evolution in turbulent flows confirm that the fluctuation dynamo action readily occurs in forced and convective turbulent flows (Meneguzzi, Frisch & Pouquet 1981; Cattaneo 1999; Haugen et al. 2003, 2004; Maron, Cowley & McWilliams 2004; Schekochihin et al. 2004), especially when $R_m \geq \text{Re}$. Such simulations are also able to follow the fluctuation dynamo into the non-linear regime where the Lorentz forces becomes strong enough to affect the flow as to saturate the growth of magnetic field.

In the kinematic regime, the field is predicted to be intermittent, i.e., concentrated into structures whose size, in at least one dimension, is as small as the resistive scale

$$l_\eta = l_0 R_m^{-1/2} \quad (18)$$

in a single-scale flow (e.g., Ruzmaikin et al. 1989; Zeldovich et al. 1990). We emphasize that magnetic field at the small Ohmic diffusion scale is produced by the shear of the flow at a larger scale l_0 .

In a turbulent flow, where a broad spectrum of motions is present, flow at each scale l would produce magnetic structures at all scales down to the corresponding Ohmic scale. In the kinematic regime this would correspond to a set of eigenfunctions, each with a distinct growth rate v_l/l . The fastest growing eigenfunction is due to stretching by the smallest eddies with $R_m(l) > R_{m,\text{cr}}$, where $R_m(l) = R_m(l/l_0)^{3/4}$. These are the viscous scale eddies, with $l = l_\nu = l_0 \text{Re}^{-3/4}$, provided $R_m/\text{Re} > R_{m,\text{cr}}$. However in the nonlinear regime, when the fastest growing mode saturates, larger scale modes could still grow. Since most of the kinetic energy is contained at the scale l_0 , the dominant magnetic scale could still be determined by dynamo action due to eddies of scale l_0 and, especially, by the subtle details of the dynamo saturation. We now discuss how the dynamo action could saturate.

Nonlinear effects can modify the resulting magnetic structures, although it is as yet not clear in what way (cf. Haugen et al. 2003, 2004; Schekochihin et al. 2004). A simple model of Subramanian (1999) suggests that the smallest scale of the magnetic structures will be renormalized in the saturated state to become

$$l_B \simeq l_0 R_{m,\text{cr}}^{-1/2}, \quad (19)$$

instead of the resistive scale l_η . This essentially happens via a renormalization of the effective magnetic diffusivity in the models of Subramanian (1999, 2003). In other words, it is suggested that the dynamo action can be saturated via a reduction of the effective magnetic Reynolds number down to its critical value for the dynamo action.¹

Such results, however plausible they are, require further substantiation, e.g., by numerical simulations. Dynamo simulations of Haugen et al. (2003, 2004) with $\nu/\eta = 1$, where $R_{m,\text{cr}} \approx 35$, show that magnetic energy per unit logarithmic interval of k , kM_k , has a broad maximum at $k \sim 9$, a scale about 6 times smaller than the forcing scale, but a factor of about four larger than the resistive scale given by $k_\eta = k_0 R_m^{1/2} \simeq (20-30)k_0$ for $R_m = 420-960$, in agreement with the above idea and Eq. (19). (We note, however, that it is not quite clear how significant is the difference or agreement here since all the estimates have factors of order unity omitted, which can be important at the modest values of R_m available.) Further, these simulations also show that the value of k_B does not scale with R_m when R_m is increased from about 420 to 960, confirming Eq. (19). However, the magnetic spectrum is rather broad and it is difficult to identify accurately the dominant magnetic scale in those simulations. Nevertheless, it is clear that the nonlinear magnetic field distribution is less intermittent (i.e., its scale is larger) than at the kinematic stage. Below we present evidence for this nonlinear behaviour in our own simulations of the fluctuation dynamo. The values of magnetic Reynolds number accessible now in such simulations are too modest to make any confident conclusions, but we believe that our approach to the saturation of the fluctuation dynamo is consistent with the evidence available.

For the Kolmogorov turbulence, in the kinematic regime, the corresponding resistive scale for the marginal mode is predicted to be $l_\eta \simeq l_0 R_m^{-3/4}$ (Subramanian 1997; Brandenburg & Subramanian 2005), when it is larger than the viscous cut-off scale (that is when $l_\eta > l_\nu = l_0 \text{Re}^{-3/4}$ or $P_m < 1$). This scaling is different from that in Eqs (18) and (19), which apply to a single-scale flow, because the shearing rate now is $(v_0/l_0)(l/l_0)^{-2/3}$ at any scale l in the inertial range. For the marginal magnetic mode (neither growing nor decaying), the shearing is balanced by dissipation at $l = l_\eta$ which occurs at a rate η/l_η^2 . In the intracluster gas, we generally have $l_\eta < l_\nu$. However in the saturated state one may have $l_B > l_\nu$ for $\text{Re} > R_{m,\text{cr}}$. This would then suggest a different scaling, $l_B \simeq l_0 R_{m,\text{cr}}^{-3/4}$ instead of Eq (19). Nevertheless, in both the simulations presented below and in real clusters the flow is not strongly turbulent, i.e., it has no extended Kolmogorov inertial range because the Reynolds number is not very large; so Eq. (19) can remain a better approximation. There is some evidence for this from the simulations, in that Eq. (19) agrees better with the wave number at which the magnetic spectrum peaks. We shall therefore use Eq. (19) in our estimates.

We note that properties of MHD turbulence can depend on the ratio $P_m = \nu/\eta$, known as the magnetic Prandtl number. The intracluster gas has $P_m \gg 1$ if Spitzer's viscosity and resistivity are adopted; realistically large values of P_m are not accessible to computer simulations, but we shall discuss simulations with a modestly large value of P_m in what follows.

can perhaps be described as a reduction of the effective magnetic Reynolds number to its critical value $R_{m,\text{cr}}$ of the kinematic dynamo, a feature which however has not yet been studied in the model of Kim (1999)

¹ Saturation could also happen if the stretching properties of the flow are suppressed by the Lorentz force (Kim 1999). This

3.2 Application to cluster turbulence

Here we present semi-quantitative estimates to characterize the fluctuation dynamo in the intracluster gas, before discussing, in Sect. 4, direct numerical simulations of the fluctuation dynamo.

3.2.1 The epoch of cluster formation

During the epoch of major mergers, we expect that the intracluster medium is involved in a steady-state, driven turbulence, for which we assume the Kolmogorov spectrum. Due to the action of eddies at scale l , the r.m.s. magnetic field grows exponentially at a rate

$$\gamma(l) = \frac{v_i}{l} = \frac{1}{t_{0i}} \left(\frac{l}{l_{0i}} \right)^{-2/3}, \quad t_{0i} \simeq \frac{l_{0i}}{v_{0i}}, \quad (20)$$

where subscript ‘i’ refers to the initial, steady state of the intracluster turbulence. As summarized in the last paragraph of Sect. 2.1, the turbulent speed and scale can be adopted as $v_{0i} = 300 \text{ km s}^{-1}$ and $l_{0i} = 150 \text{ kpc}$, respectively. Assuming that the driven turbulence lasts for $t_f = 3 \text{ Gyr}$, we obtain an amplification exponent of the magnetic field $\Gamma = \gamma(l)t_f \approx 6$ at $l = l_{0i}$ (and larger at smaller scales). So the seed field can be amplified by a factor 400 by motions at $l = l_{0i}$ during this time (the amplification factor is larger at smaller scales). For a seed magnetic field of 10^{-8} G , this amplification is sufficient to explain the observed magnetic fields; this implies that the observed magnetic fields are plausibly in the saturated state and the Lorentz force can now affect significantly the velocity field in galaxy clusters.

3.2.2 The epoch of decaying turbulence

After the driving forces have been diminished, the turbulence decays. Both the instantaneous outer scale and the viscous scale then increase with time (the latter, because of the decrease in the Reynolds number). In this situation it is more useful to estimate the growth rate at a fixed scale l , which belongs to the turbulent spectrum for a long time and can hence lead to a fluctuation dynamo, instead of considering an evolving viscous scale (where the dynamo time scale is the shortest). The instantaneous growth rate of the r.m.s. magnetic field due to motions at a fixed scale l decreases with time as

$$\begin{aligned} \gamma(l, t) &= \frac{v_l(t)}{l} \\ &= \frac{v_{li}}{(l^2 l_{0i})^{1/3}} \left(\frac{t - t_f}{t_{0i}} \right)^{-\left(\frac{1}{2}\alpha + \frac{1}{3}\beta\right)}, \quad t \gg t_{0i}. \end{aligned} \quad (21)$$

Here we have adopted a Kolmogorov spectrum with $v_l = v_0(t)[l/l_0(t)]^{1/3}$ and for numerical estimates take $\alpha = 6/5$ and $\beta = 2/5$. For a growth rate evolving with t , magnetic field evolves as $B \propto \exp \int_0^t \gamma(l, t') dt'$. If turbulence is maintained in a steady state during an initial period $t \leq t_f$ and then γ decreases as in Eq. (21), the amplification exponent for the Kolmogorov spectrum follows as

$$\int_0^t \gamma(l, t') dt' = \Gamma(t) \left(\frac{l}{l_{0i}} \right)^{-2/3}, \quad (22)$$

where

$$\Gamma(t) = \begin{cases} \frac{t}{t_{0i}}, & t \leq t_f + t_{0i}, \\ 1 + \frac{t_f}{t_{0i}} + \frac{1}{\zeta} \left[\left(\frac{t - t_f}{t_{0i}} \right)^\zeta - 1 \right], & t > t_f + t_{0i}, \end{cases}$$

where $\zeta = 1 - \frac{1}{2}\alpha - \frac{1}{3}\beta$. We have applied the power-law (21) only at $t > t_f + t_{0i}$ and assumed that the decay does not affect the growth rate before that time. Assuming that the turbulence starts decaying after a time $t_f = 3 \text{ Gyr}$, we obtain, at $t = 5 \text{ Gyr}$, that the energy-range speed reduces down to $v_0 \approx 130 \text{ km s}^{-1}$, whereas the energy-range scale increases to $l_0 \approx 260 \text{ kpc}$. The amplification exponent of magnetic field due to motions at $l = l_{0i}$ is obtained as $\Gamma \approx 9$ at $t = 5 \text{ Gyr}$ (consisting of 7 at $t = t_f + t_{0i} = 3.5 \text{ Gyr}$ and only less than 2 at later times), so that the seed field could be amplified by a factor about 6×10^3 by the end of the decay phase if it were too weak to bring the dynamo to the saturated state earlier. In order to obtain magnetic field of $1 \mu\text{G}$ at this scale for $t = 5 \text{ Gyr}$, a seed field of $2 \times 10^{-10} \text{ G}$ would be sufficient. Again the amplification is larger due to smaller scale eddies which remain part of the turbulent cascade as the turbulence decays.

3.2.3 Dynamo action in wakes

Using the turbulent speed and scale averaged over the wake length, as derived in Sect. 2.3.2, we obtain magnetic field growth time scales $\gamma^{-1} \simeq l_0/v_0 \simeq 0.8 \text{ Gyr}$ for subcluster wakes and $3 \times 10^7 \text{ yr}$ for galactic wakes. At a given position, time available for the dynamo action is X/V_i , where $V_i \simeq 1000 \text{ km s}^{-1}$ is the speed of a subcluster or a galaxy. Therefore, the dynamo amplification exponent is given by

$$\Gamma \simeq \frac{v_0}{V_i} \frac{X}{l_0} \simeq 3$$

for both subclusters and galaxies, which implies additional amplification by a factor 20 at the outer scale.

3.2.4 Magnetic field strength in the intracluster gas

The maximum local magnetic field strength produced by the turbulent dynamo will be, presumably, close to equipartition with the turbulent energy:

$$\begin{aligned} B_{\text{eq}} &= (4\pi\rho v_0^2)^{1/2} \\ &\simeq 3 \mu\text{G} \left(\frac{n}{10^{-3} \text{ cm}^{-3}} \right)^{1/2} \left(\frac{v_0}{200 \text{ km s}^{-1}} \right), \end{aligned} \quad (23)$$

where ρ is the gas density. [We note that some models of nonlinear fluctuation dynamo predict stronger local magnetic fields (Belyanin et al. 1993, 1994), but here we adopt a conservative limit (23).] As discussed in Sect. 3.1, magnetic field produced by the fluctuation dynamo is expected to be spatially intermittent (especially at early stages of dynamo action), i.e., represented by intense filaments and sheets whose volume filling factor is less than unity. Numerical simulations and analytical models recently reviewed by Brandenburg & Subramanian (2005) suggest that magnetic sheets and ribbons are prevalent, whose thickness is given by Eq. (19) and whose other two dimensions are of the order of the turbulent scale l_0 (see Fig. 5). Then the volume filling factor of magnetic structures *within a single turbulent cell* in the statistically steady state can be estimated as

$$f_B = \frac{l_B l_0^2}{l_0^3} \simeq R_{m,cr}^{-1/2} \approx 0.17,$$

where the numerical value refers to $R_{m,cr} = 35$. Therefore, the r.m.s. magnetic field within a turbulent cell is of order

$$\begin{aligned} \langle B^2 \rangle^{1/2} &\simeq f_B^{1/2} B_{eq} \\ &\simeq 1.2 \mu\text{G} \left(\frac{n}{10^{-3} \text{ cm}^{-3}} \right)^{1/2} \left(\frac{v_0}{200 \text{ km s}^{-1}} \right) \\ &\quad \times \left(\frac{R_{m,cr}}{35} \right)^{-1/4}, \end{aligned} \quad (24)$$

which implies that magnetic energy density in a saturated dynamo state is a factor $R_{m,cr}^{1/2} \simeq 6$ times smaller than the turbulent energy density. (Here and below angular brackets denote averaging.) We emphasize that weaker volume-filling magnetic fields are also present; their contribution to the magnetic energy density can be somewhat smaller than that of the intermittent part. In agreement with this estimate, magnetic energy density is about 0.2 (0.33) of the kinetic energy density in Model 1 (Model 2) of the numerical simulations discussed in Sect. 4. As discussed by Haugen et al. (2004, their Fig. 14), this ratio weakly varies with magnetic Reynolds number; in their simulations, the variation is from about 0.25 for $R_m = 420$ to 0.4 for $R_m = 960$, both with $P_m = 1$. For $P_m = 30$, their simulations yield the magnetic-to-kinetic energy ratio of about unity. Thus, the flow at larger magnetic Prandtl number appears to be producing more magnetic energy; perhaps magnetic structures fill turbulent cells more densely, and/or a smoothly distributed magnetic field is stronger. This feature is yet to be understood. What is, however, important for our immediate purpose here, is that the fluctuation dynamo produces magnetic fields whose energy density is comparable to the kinetic energy density of the turbulence.

If the volume filling factor of the turbulent flow f_V is less than unity, as in the case of turbulent wakes of sub-clusters and galaxies, the r.m.s. magnetic field in the cluster volume is obtained from Eq. (24) by further multiplication by a factor $f_V^{1/2}$; this is a measure of the total magnetic energy of the cluster. However, this quantity has little physical significance because it would not result from any local magnetic measurement. In this sense, the local value (24) is more meaningful; it is presented in Table 1 together with other quantities that characterize turbulence and magnetic fields at various stages of the cluster evolution.

4 SIMULATIONS OF THE FLUCTUATION DYNAMO

We have simulated the generation and subsequent decay of dynamo-active turbulence using the numerical model of the fluctuation dynamo by Haugen et al. (2003, 2004), where isothermal, viscous, electrically conducting, compressible gas is driven by a random force imposed as a source in the Navier–Stokes equation. The Navier–Stokes, continuity and induction equations are then solved in a Cartesian box of a size D on a cubic grid with 256^3 mesh points. The driving force \mathbf{f} is sinusoidal in the spatial coordinates, transversal ($\mathbf{f} \perp \mathbf{k}$ with \mathbf{k} the wave vector of the force), and localized in the wave-number space about a certain wave number $k = k_f$, so it drives almost incompressible, vortical motions in a cer-

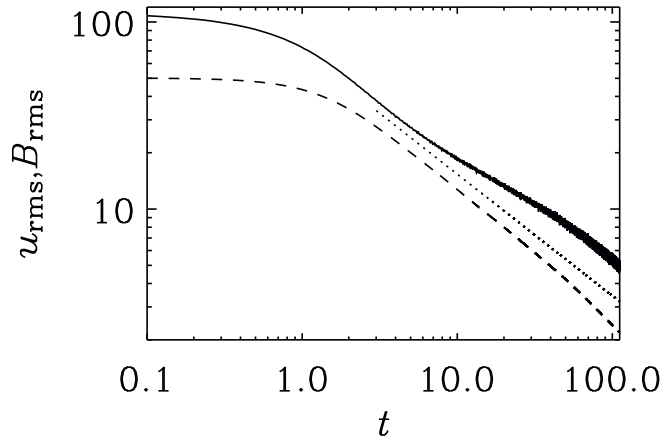


Figure 2. The evolution of the r.m.s. fluid velocity (solid) and magnetic field (dashed) in driven and then decaying turbulence with $\tilde{k}_f = 5$ (Model 1) ($v_{rms} \equiv \langle v^2 \rangle^{1/2}$ and likewise for B). Velocity is measured in the units of diffusive speed at the driving wavelength, νk_f , and magnetic field is expressed in similar velocity units, $(4\pi\rho)^{1/2} c_s \nu k_f$. Hence, v_{rms} numerically coincides with Re in the statistically steady state. Time is measured in the units of the initial turnover time of the energy-containing eddies, t_{0i} . Dotted line shows the asymptotics $(t - t_f)^{-0.65}$, where $t_f = 0$ is the time when the forcing is turned off.

tain wavelength range around $2\pi/k_f$ (see Haugen et al. 2004 for details). The direction of the wave vector of the force and its phase change randomly every time step in the simulations, so the force is effectively δ -correlated in time.

We represent numerical results using the following units. (Tilde is used to denote dimensionless quantities.) For a unit length d , the computational domain size is equal to $D = 2\pi d$. The wave number is measured in the units of d^{-1} . In simulations with dimensionless forcing wave number \tilde{k}_f , it is appropriate to adopt $k_f = 2\pi/l_0$ for its dimensional value, where $l_0 = 150$ kpc is the turbulent scale in a merging cluster, as obtained in Sect. 2.1. Then the unit length is $d = \tilde{k}_f l_0 / (2\pi)$ and the dimensional size of the computational domain is $D = l_0 \tilde{k}_f$. The unit density ρ_0 can be adopted to correspond to the number density of $n_0 = 10^{-3} \text{ cm}^{-3}$. The unit speed is the speed of sound, $c_s = 1000 \text{ km s}^{-1}$, so that the unit magnetic field is $(4\pi\rho_0)^{1/2} c_s = 15 \mu\text{G}$.

Here we report results obtained with two values of the central driving wave number k_f . Some results were obtained with driving covering the range of dimensionless wave numbers $\tilde{k} = 4.5\text{--}5.5$, centred at $\tilde{k}_f = 5$ (Model 1). Results at higher resolution (which was especially needed when $P_m > 1$), were obtained with the driving wave-number range of $\tilde{k} = 1\text{--}2$ centred at $\tilde{k}_f = 1.5$ (Model 2). In these latter runs, the computational box contains just a few turbulent cells.

The intensity of the driving was adjusted to obtain the r.m.s. Mach number of the turbulence of about 0.1 which produces relative density fluctuations of order 0.01 (implying that only a small fraction of the total velocity is compressible). The kinematic viscosity and magnetic diffusivity in most runs are adopted to be equal to $\nu = \eta = 2 \times 10^{-4} c_s d$ (i.e., a magnetic Prandtl number of unity). This corresponds to $Re = R_m \approx 110$ in Model 1 and $Re = R_m \approx 420$ in Model 2, which is close to what is expected for Re in the

Table 1. Summary of turbulence and magnetic field parameters at various stages of cluster evolution: duration of the stage (the last two stages represent steady states), the r.m.s. velocity v_0 and scale l_0 of turbulence and eddy turnover time t_0 (for the decaying turbulence, values for the middle of the decay stage are given, 2 Gyr after its start), the equipartition magnetic field B_{eq} given by Eq. (23) (i.e., maximum field strength within a turbulent cell), thickness of magnetic filaments and sheets l_B , defined in Eq. (19), for the statistically steady state of the dynamo, the r.m.s. magnetic field within a turbulent cell $B_{\text{rms}} \equiv \langle B^2 \rangle^{1/2}$ given by Eq. (24) (the latter two obtained for $R_{\text{m,cr}} = 35$), and finally the standard deviation of the Faraday rotation measure σ_{RM} [calculated using Eq. (28) for the volume filling turbulence within 500 kpc of the centre and path length of 750 kpc in the first two lines, and assuming one transverse wake along the line of sight in the last two lines, using Eq. (30)]. Subcluster mass of $3 \times 10^{13} M_{\odot}$ has been assumed.

Evolution stage	Duration [Gyr]	v_0 [km s ⁻¹]	l_0 [kpc]	t_0 [Gyr]	B_{eq} [μG]	l_B [kpc]	$\langle B^2 \rangle^{1/2}$ [μG]	σ_{RM} [rad m ⁻²]
Major mergers	4	300	150	0.5	4	25	1.8	200
Decaying turbulence	5	130	260	2.0	2	44	0.8	120
Subcluster wakes		260	200	0.8	4	34	1.6	110
Galactic wakes		300	8	0.03	4	1.4	1.6	5

intracluster gas. (We note, however, that the values of magnetic Reynolds number explored here still are smaller than those expected in reality.) We have also considered the case where magnetic diffusivity is 30 times smaller than kinematic viscosity in runs with $\tilde{k}_f = 1.5$, $\nu = 1.5 \times 10^{-3} c_s d$ and $\eta = \nu/30$, i.e., $P_m = 30$, $\text{Re} \approx 44$ and $R_m \approx 1300$. Results presented in what follows refer to the case $P_m = 1$ unless stated otherwise.

In order to simulate dynamo action in forced and then decaying turbulence, the flow had been driven until it reached a statistically steady state, with a weak magnetic field introduced at the start of the simulation. Then the system was evolved for some period (about 45 time units in Model 1), after which the driving force was switched off; $t_f = 0$ is the time when the driving halts. The initial, weak magnetic field is random, with energy density of about 0.6% of the kinetic energy density in Model 1.

Figure 2 shows the time evolution of the suitably normalized r.m.s. velocity and magnetic field obtained in Model 1, after the driving was switched off [in fact, $v_{\text{rms}}/(\nu \tilde{k}_f)$, shown with solid line, is the Reynolds number based on the forcing scale, with $v_0 \approx v_{\text{rms}}$]. The initial exponential growth of the r.m.s. magnetic field that obtains (not shown in Figure 2), is followed by its saturation at a level where its energy density is about 0.2 (0.3) of the turbulent energy density in Model 1 (Model 2). More precisely, the r.m.s. values of the turbulent velocity and magnetic field (measured in velocity units) in the steady state of Fig. 2 are about $0.114 c_s$ and $0.050 c_s$, respectively, whereas the similar quantities for $\tilde{k}_f = 1.5$ are $0.116 c_s$ and $0.065 c_s$. The critical value of the magnetic Reynolds number remains about 35 in both models.

The subsequent decay of both the velocity and magnetic field strength can be approximated by $(t - t_f)^{-0.65}$ for $t \gg t_{0i}$, as shown with dotted line. This decay law is consistent with Eq. (4) which predicts the power law exponent of $-3/5$. However, the alternative value $\alpha = 10/7$ would result in the exponent of $-5/7 \approx -0.71$, which is also consistent with our numerical results.

With $l_0 = 150$ kpc and $n = 10^{-3} \text{ cm}^{-3}$, the r.m.s. turbulent velocity and magnetic field strength in the steady state in Fig. 2 are $\langle v^2 \rangle^{1/2} \approx 110 \text{ km s}^{-1}$ and $\langle B^2 \rangle^{1/2} \approx 0.7 \mu\text{G}$, respectively. These results favourably agree with estimates

presented in Table 1 in the sense that in both cases the ratio of the turbulent and Alfvén speeds is about 1/2, which confirms our estimate of the r.m.s. magnetic field strength in Eq. (24). In other words, if our simulations had stronger driving to achieve $\langle v^2 \rangle^{1/2} \approx 300 \text{ km s}^{-1}$, then the r.m.s. magnetic field would be $\langle B^2 \rangle^{1/2} \approx 2 \mu\text{G}$, as in our analytical estimate.

The magnetic and kinetic energy spectra are shown in Fig. 3. In the statistically steady state (the upper curves), kinetic energy in Model 1 peaks at $\tilde{k}_f = 5$, the driving wave number. However, magnetic energy has broad maximum at a significantly smaller scale, apparently because of its intermittent structure. This difference is better visible in the right panel that refers to Model 2 where we have higher resolution. Similar simulations, but with a significantly higher resolution 1024^3 (Haugen et al. 2003, 2004), confirm that the magnetic energy per unit logarithmic interval in the k -space, kM_k , has a maximum at $k_B \approx 6\tilde{k}_f$ in excellent agreement with Eq. (19) with $R_{\text{m,cr}} = 35$, but no significant dependence of k_B on R_m has been revealed. The value of R_m in those simulations is about 1000, so the deviation from the scaling $k_B \sim k_\eta \propto R_m^{-1/2}$ advocated by Schekochihin et al. (2004) is by a factor of 3–5 over the range $R_m = 400$ –1000.

The length scales of the velocity and magnetic fields can be characterized more precisely in terms of their integral scales

$$L_v = 2\pi \frac{\int k^{-1} E_k dk}{\int E_k dk}, \quad (25)$$

and similarly for the magnetic scale L_B ; here integration extends over the whole interval of k available. These scales are simply related to the longitudinal l_L and transverse l_N integral scales of the magnetic fields by $l_L = \frac{1}{2} l_N = \frac{3}{8} L_B$ [Eq. (12.91) of Monin & Yaglom 1975], and similarly for L_v , but only approximately because \mathbf{v} is not solenoidal. The dimensionless value of the longitudinal integral scale of magnetic field in the steady state is then obtained from Fig. 4 as $l_B = \sqrt{2/\pi} l_L \approx 0.16$ (see Appendix B). This agrees reasonably well with the prediction from our heuristic estimates, $l_B \simeq (2\pi/\tilde{k}_F) R_{\text{m,cr}}^{-1/2} \simeq 0.2$. The time variation of these scales is shown in Fig. 4. When the turbulence decays, the integral scales of both velocity and magnetic field exhibit power-law

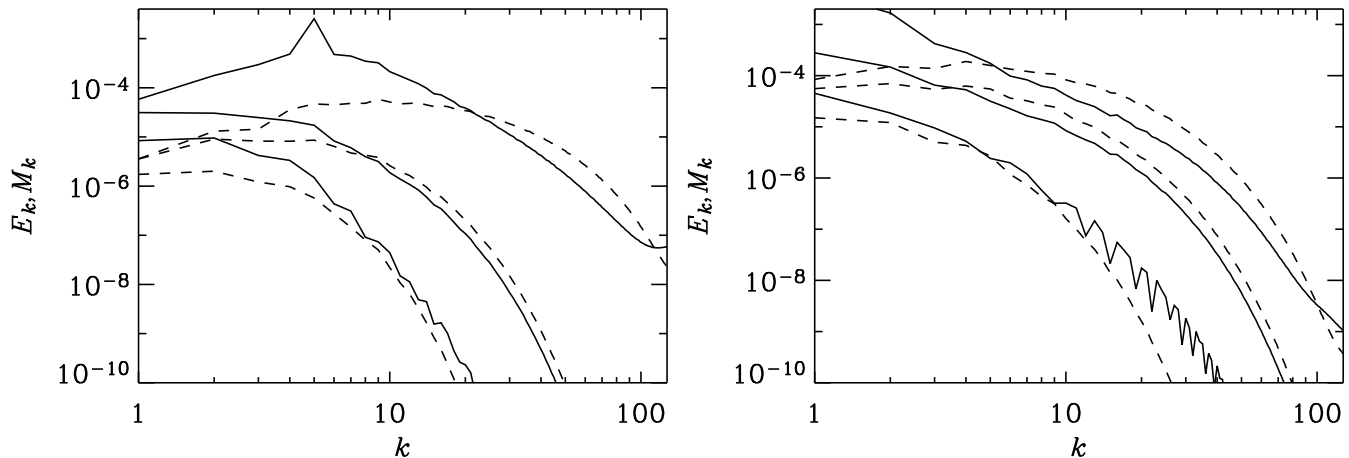


Figure 3. The energy spectra of kinetic (solid) and magnetic (dashed) energies at various stages of evolution, $t/t_{0i} = 0, 10, 50$, with (a) $\tilde{k}_f = 5$ – Model 1, left panel, and (b) $\tilde{k}_f = 1.5$ – Model 2, right panel. Spectra obtained at later times are at lower levels because of the decay of turbulent energy.

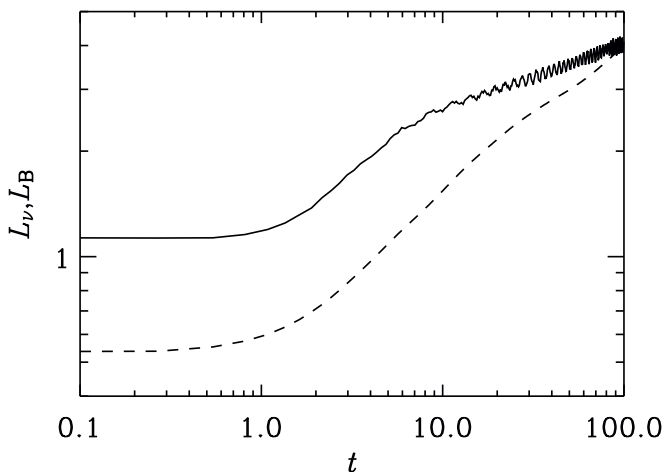


Figure 4. Evolution of the integral scales of the velocity (L_v , solid line) and magnetic fields (L_B , dashed line), as defined in Eq. (25), with $\tilde{k}_f = 5$ (Model 1).

increase, in agreement with Eq. (4); the growth slows down when L_v has grown to become comparable with the box size.

Magnetic energy at small scales has, at early times, excess over kinetic energy because magnetic field is very intermittent, which is especially clearly visible in the right panel of Fig. 3. At later stages, magnetic field distribution becomes more homogeneous and this feature disappears. Simultaneously, the scale of magnetic field increases and becomes comparable to that of the flow, which is not the case at early stages.

Figure 5 illustrates (using Model 2) the structure of magnetic field in a turbulent flow in a statistically steady state (left panel) and at a late stage of decay (right panel). The magnetic field produced by the fluctuation dynamo consists of an intermittent part, represented by randomly distributed, intense magnetic ribbons, sheets and filaments (which can even be folded), immersed in a sea of volume-filling random magnetic field. The intermittency gradually reduces as the turbulence decays together with magnetic field because structures of smaller scale decay faster, and the

volume filling factor of magnetic field increases with time – this tendency can easily be seen in the right panel of Fig. 5.

5 OBSERVATIONAL DIAGNOSTICS

5.1 The Faraday rotation measure

An important observational diagnostic of the intracluster magnetic field is the Faraday rotation of polarized radio emission of background sources (located beyond the cluster or in its centre) produced in the intracluster gas. The Faraday rotation is quantified by the Faraday rotation measure

$$\text{RM} = K \int_L n_e \mathbf{B} \cdot d\mathbf{l}, \quad (26)$$

where n_e is the number density of free thermal electrons, the integral is taken along the path length L from the source to the observer, and $K = 0.81 \text{ rad m}^{-2} \text{ cm}^3 \mu\text{G}^{-1} \text{ pc}^{-1}$. For a magnetic field with zero mean value $\langle \mathbf{B} \rangle = 0$, the mean value of RM vanishes, whereas its standard deviation can be represented in the form (Appendix B; see also Burn 1966; Sokoloff et al. 1998),

$$\sigma_{\text{RM}} \simeq \text{RM}_0 \sqrt{N}, \quad (27)$$

where RM_0 is the Faraday rotation measure produced in a single turbulent cell of a size l_0 and $N = L/l_0$ is the number of the cells along the line of sight.

Suppose that each turbulent cell contains randomly oriented magnetic sheets of thickness l_B where magnetic field strength is equal to B_{eq} , with a covering factor of order unity, as described in Sect. 3.2.4. Then the Faraday rotation measure produced in a single turbulent cell follows as $\text{RM}_0 \simeq K n_e B_{\text{eq}} l_B$, and, adopting $l_B = l_0 R_{\text{m,cr}}^{-1/2}$,

$$\begin{aligned} \sigma_{\text{RM}} &\simeq K n_e B_{\text{eq}} R_{\text{m,cr}}^{-1/2} (l_0 L)^{1/2} \\ &\simeq 110 \frac{\text{rad}}{\text{m}^2} \left(\frac{n_e}{10^{-3} \text{ cm}^{-3}} \right) \left(\frac{B_{\text{eq}}}{3 \mu\text{G}} \right) \left(\frac{R_{\text{m,cr}}}{35} \right)^{-1/2} \\ &\quad \times \left(\frac{l_0}{100 \text{ kpc}} \right)^{1/2} \left(\frac{L}{750 \text{ kpc}} \right)^{1/2}. \end{aligned} \quad (28)$$

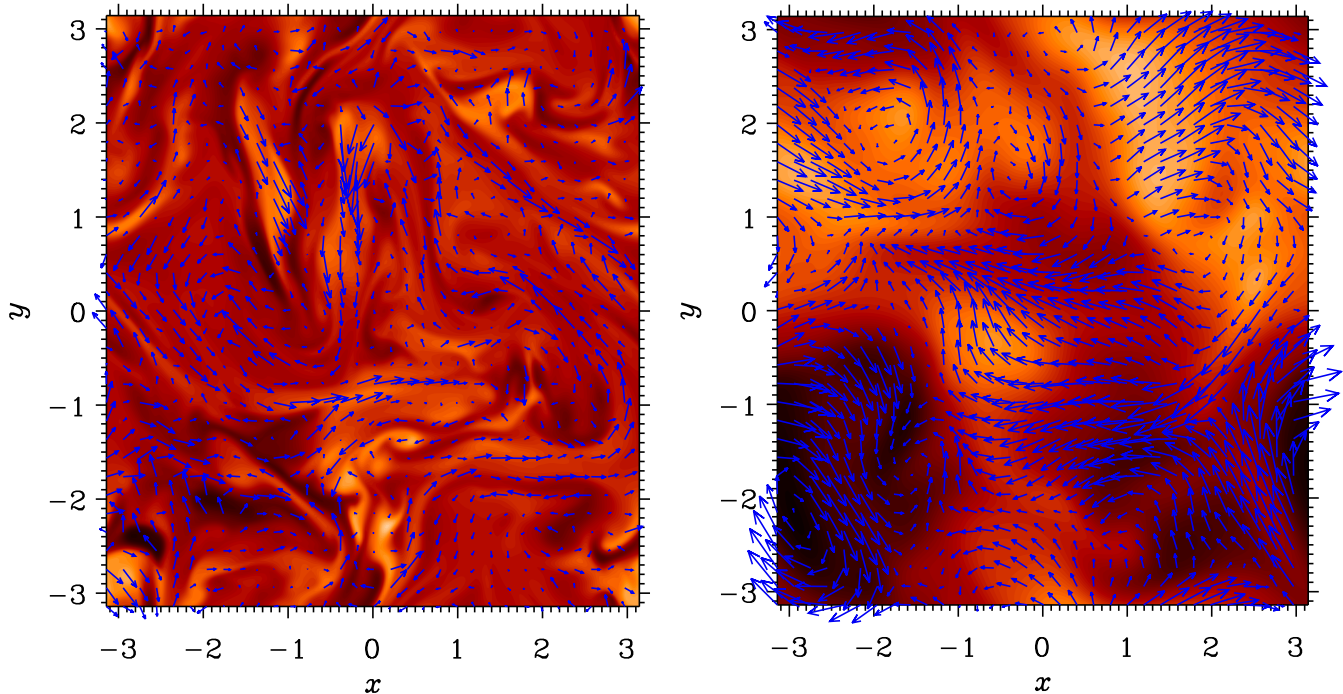


Figure 5. Snapshots of magnetic field in a cross-section through the middle of the computational domain of Model 2 at $t/t_{0i} = 0.30$ when the system is in a statistically steady state (left panel), and $t/t_{0i} = 59.34$, at a late stage of decay (right panel). Here $k_f = 1.5$, so each frame contains a few turbulent cells. The magnitude of the field component perpendicular to the plane of the figure is shown color coded (in shades of grey) with black corresponding to field pointing into the figure plane, and lighter shades, to field pointing out of the plane. The field in the plane of the figure is shown with vectors whose length is proportional to the field strength.

If the magnetic sheets multiply cover the projected area a turbulent cell, by a factor $q = O(1)$, then additional factor $q^{1/2}$ has to be included in Eq. (28). The comparison of Eq. (28) with both numerical simulations and observations of Faraday rotation in galaxy clusters suggest that $q \approx 1$. If $B_{\text{eq}} \propto v_0 \propto t^{-3/5}$ and $l_0 \propto t^{2/5}$, the observed RM will, on average, decrease with time as

$$\sigma_{\text{RM}} \propto [(t - t_f)/t_{0i}]^{-2/5}. \quad (29)$$

We have calculated the Faraday rotation measure for 256^2 lines of sight through our computational domain, and then computed σ_{RM} as the standard deviation of the results. The evolution of σ_{RM} in decaying turbulence is shown in Fig. 6 for Model 1 and it exhibits remarkable agreement with Eq. (29). At earlier stages of the simulations in Model 1, σ_{RM} first grows rapidly while magnetic field is exponentially amplified, and then remains fairly constant, $\sigma_{\text{RM}} \approx 0.3$, for $-20 < t < 1$ (Fig. 6). In dimensional units, this corresponds to $\sigma_{\text{RM}} \approx 80 \text{ rad m}^{-2}$. Model 2 results in a value of $\sigma_{\text{RM}} \approx 0.47$ (Fig. 8), corresponding to 130 rad m^{-2} .

It is useful to compare results of the simulations with the analytical estimate of Eq. (28), $\bar{\sigma}_{\text{RM}} \simeq (B_{\text{eq}}/\langle B^2 \rangle^{1/2}) R_{\text{m,cr}}^{-1/2} \tilde{k}_f^{1/2}$ in dimensionless units used in Fig. 6. This gives $\bar{\sigma}_{\text{RM}} \simeq 0.4$ for $\tilde{k}_f = 1.5$ in Model 2 and $\bar{\sigma}_{\text{RM}} \simeq 0.75$ for $\tilde{k}_f = 5$ in Model 1. This estimate of $\bar{\sigma}_{\text{RM}}$ for Model 2, which has a higher spatial resolution, is in good agreement with the numerical simulations, but that obtained for Model 1 is a factor of about 2 lower than expected. Nevertheless, our simulations confirm that Eq. (28) and Table 1 provide reasonably good estimates of the expected amount

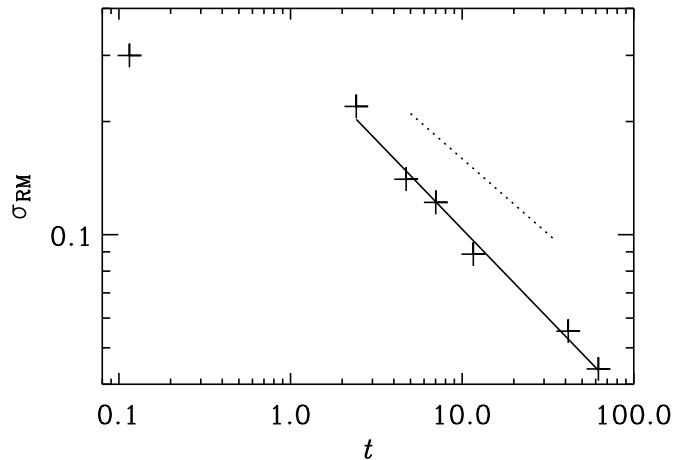


Figure 6. The width of the histogram of Faraday rotation measures, σ_{RM} , calculated along 256^2 lines of sight through the computational box, with $\tilde{k}_f = 5$ (Model 1, as in Fig. 2), as a function of time. The solid line is the least square fit to the data points at $t > 1$, while the dotted line corresponds to $t^{-2/5}$. Here σ_{RM} is measured in the units $Kn_e(B^2)^{1/2}l_0 \approx 280 \text{ rad m}^{-2}$, so that $\sigma_{\text{RM}} \approx 80 \text{ rad m}^{-2}$ in the steady state.

of Faraday rotation by magnetic field generated by the fluctuation dynamo.

Altogether the estimate (28) and the amount of Faraday rotation in our simulations agree very well with observations of Faraday rotation in the intracluster gas.

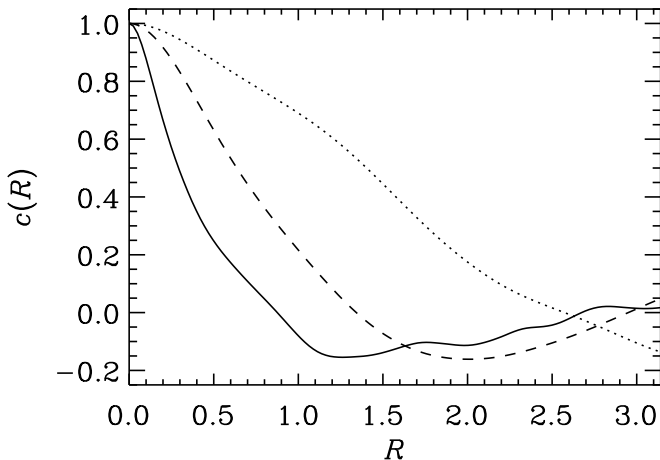


Figure 7. The normalized autocorrelation function $c(R) = C(R)/\sigma_{\text{RM}}^2$, where $C(R) = \langle \text{RM}(\mathbf{X} + \mathbf{R})\text{RM}(\mathbf{X}) \rangle$ and $\sigma_{\text{RM}}^2 = \langle \text{RM}^2(\mathbf{X}) \rangle$ obtained for Model 2 ($k_f = 1.5$) with $P_m = 1$, at various times: $t = 0$ (solid), $t = 30$ (dashed) and $t = 70$ (dotted). The former curve refers to the statistically steady state, whereas the latter two illustrate how RM distribution becomes less intermittent as turbulence decays. Here R is measured in the units of $\tilde{k}_f l_0 / (2\pi) \approx 70$ kpc.

Figure 7 shows the autocorrelation function of the Faraday rotation measure for Model 2 at the beginning of the evolution and at two later times. As turbulence decays and magnetic field becomes less structured, the correlation scale of RM fluctuations increases. In the steady state, the dimensional value of the Taylor microscale (or differential length scale) of the RM fluctuations is, as expected, about $R_{\text{RM}} \approx 15$ kpc, i.e., about half the thickness of magnetic sheets, l_B , as quoted in Table 1.

The situation is somewhat different for the wakes of subclusters and individual galaxies. As discussed in Sects 2.3.3 and 2.3.4, their volume filling factor is small, whereas the area covering factor can be of order unity. In other words, a line of sight typically passes through just a single turbulent wake, where the turbulent scale is comparable to the wake width. The resulting Faraday rotation measure is given by

$$\begin{aligned} \sigma_{\text{RM}} &= K n_e B_{\text{eq}} l_B \\ &\simeq 8.6 \frac{\text{rad}}{\text{m}^2} \left(\frac{n_e}{10^{-3} \text{ cm}^{-3}} \right) \left(\frac{B_{\text{eq}}}{1 \mu\text{G}} \right) \left(\frac{l_B}{10 \text{ kpc}} \right), \quad (30) \end{aligned}$$

where we retain the notation σ_{RM} because the resulting amount of Faraday rotation will remain random, both because of the random orientation of the wakes and due to the randomness of magnetic field within the wake.

Estimates of typical Faraday rotation measures obtained from Eqs (28) and (30) are given in the last column of Table 1.

Schekochihin et al. (2005a,b) suggest a different spatial structure of the cluster magnetic field, based on their interpretation of the fluctuation dynamo for $P_m \gg 1$ (Schekochihin et al. 2004). These authors suggest that magnetic field produced by the dynamo is locally anisotropic and represents l_0 -long magnetic sheets and/or ribbons multiply folded at a microscopic resistive scale l_η . Such a model would typically produce a much smaller σ_{RM} . Arguments similar to those that lead to Eq. (28), (even assuming that the folds are

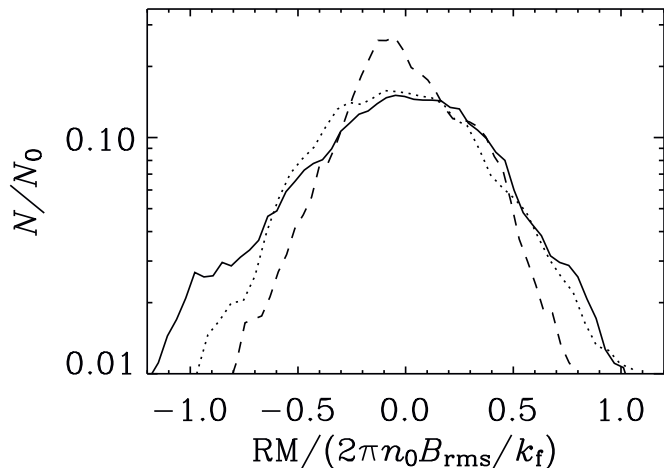


Figure 8. The histogram (probability density) of the Faraday rotation measure calculated along 256² lines of sight through the computational box, with $k_f = 1.5$, for $P_m = 1$ (solid), $P_m = 30$ (dashed) and $P_m = 1/4$ (dash-dotted), all in the statistically steady state before the decay starts, and with $\text{Re} = 450, 44, 445$ respectively. Here RM is normalized by $K n_e \langle B^2 \rangle^{1/2} l_0$, with $B_{\text{rms}} \equiv \langle B^2 \rangle^{1/2}$.

randomised by some unspecified mechanism) predict σ_{RM} smaller than in our model by a factor $F \simeq (R_m/R_{m,\text{cr}})^{1/2}$. In our simulations, this corresponds to $F \simeq 3\text{--}5$ over the range $R_m = 400\text{--}1000$. So the simulations that we have analysed (with $R_m \simeq 400$), cannot help to confidently discriminate between the two magnetic field geometries.

However, observations indicate that magnetic coherence scale is at least a few kpc and more plausibly exceed 10 kpc. This would be difficult to produce in the model of Schekochihin et al. (2005a,b), unless the effective value of R_m in the clusters is reduced, say due to plasma effects, to be close to $R_{m,\text{cr}}$. Furthermore, Schekochihin et al. (2005a,b) envisage systematic reversals of the folded magnetic field along the line of sight, rather than random changes of its direction. Such a systematic behaviour would reduce σ_{RM} even further due to systematic cancellations of magnetic field along the line of sight which would preclude the random walk of the polarization angle assumed in Eq. (28).

We have also used numerical simulations to examine the effects of varying the magnetic Prandtl number on magnetic field structure and Faraday rotation. The probability distribution of the Faraday rotation measure along 256² lines of sight through the computational box is shown in Fig. 8 for three values of the magnetic Prandtl number. The shape of the probability distribution is close to a Gaussian curve for $P_m = 1/4$ and $P_m = 1$ (which is a parabolic shape in this representation), but the distribution obtained at $P_m = 30$ exhibits shorter tails at large $|\text{RM}|$. The reason for this is apparently the abundance of small-scale structures that produce smaller Faraday rotation when $P_m \geq 1$, i.e., when the magnetic dissipation scale is smaller. Nevertheless, the standard deviation of the Faraday rotation measure has similar values for both $P_m = 1$ and $P_m = 30$, $\sigma_{\text{RM}} \approx 0.47$ and 0.3 in the units of Fig. 8, respectively. This implies that magnetic field does not become more strongly folded as P_m increases. For the reader's convenience, we note again that $\text{Re} \approx 44$

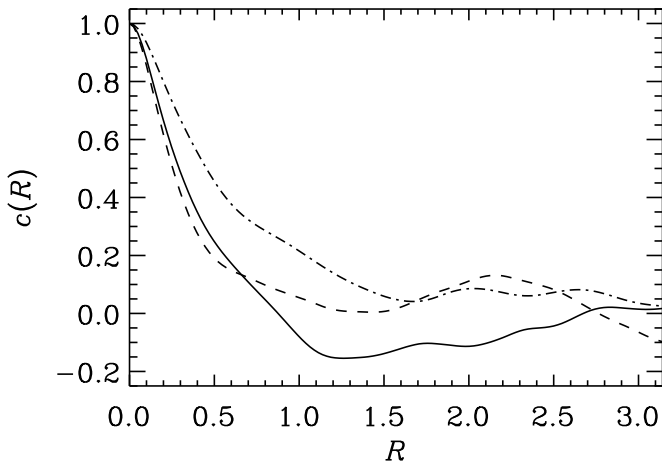


Figure 9. As in Fig. 7, but for different magnetic Prandtl numbers; $P_m = 1$ (solid), $P_m = 30$ (dashed) and $P_m = 1/4$ (dotted), all in the statistically steady state with $\tilde{k}_f = 1.5$ before the decay starts.

and $R_m \approx 1300$ for $P_m = 30$ and $Re \approx 445$ and $R_m \approx 111$ for $P_m = 1/4$.

Figure 9 shows the autocorrelation function of the Faraday rotation measure for various values of P_m . The correlation scales for both $P_m = 30$ and $P_m = 1$ are comparable, but that which obtains when $P_m = 1/4$ is a factor of two larger.

We emphasize again that both the form of the RM probability distribution and the correlation function do not change much as P_m increases from unity to 30. This suggests that our results can be robust and directly comparable with observations even though $P_m \gg 1$ in the intracluster gas. Nevertheless, it would be important to clarify this issue further using simulations with higher resolution. Note that the Faraday rotation measure is proportional to the product of magnetic field and its scale; therefore, it remains dominated by large scales for magnetic spectra $M_k \propto k^\kappa$ with $\kappa < 1$.

5.2 Polarization of cluster radio halos

Estimates of the scale of magnetic field in galaxy clusters obtained above are somewhat larger than what is usually adopted. We predict that the number of turbulent correlation cells along a path length of 750 kpc can be only about 3–5. As discussed above, magnetic field in each cell has an intermittent component of randomly oriented sheets and somewhat weaker fields in a volume filling component (see Fig. 5). It can be expected that synchrotron emission produced in such a random magnetic field will be significantly polarized (assuming that magnetic field is well ordered within individual magnetic sheets). As discussed by Sokoloff et al. (1998, their Sect. 5.1), the expected degree of polarization is a random quantity whose standard deviation is about

$$\sigma_p \simeq p_0 N^{-1/2},$$

where $p_0 \approx 70\%$ is the intrinsic degree of polarization and N is the number of turbulent cells within the beam cylinder, which yields $\sigma_p \simeq 30\%$, neglecting beam depolarization (see below). (We note that this estimate strictly applies if $N \gg$

1.) The polarized emission would be confined to elongated structures (cross-sections of magnetic sheets) of $l_B = 20$ –40 kpc in width and $l_0 = 150$ –300 kpc in length. The intrinsic polarization plane should be perpendicular to the major axes of the elongated synchrotron structures since magnetic field is mostly parallel to the magnetic sheets.

However, the fractional polarization observed from cluster radio halos is less than 2–10% at the wavelength $\lambda = 21$ cm (L. Feretti 2003, private communication; Govoni & Feretti 2004). No significant diffuse polarized emission in the Coma cluster has been detected by Thierbach, Klein & Wielebinski (2003) at wavelengths $\lambda 11.2$ cm and $\lambda 6.2$ cm. The depolarization can be attributed to internal Faraday dispersion by the random magnetic field, where the degree of polarization will be further reduced to [Eq. (34) of Sokoloff et al. 1998]

$$p = \sigma_p \frac{1 - \exp(-S)}{S}, \quad S = 2\lambda^4 \sigma_{\text{RM}}^2$$

(which is strictly applicable when $N \gg 1$). Faraday dispersion readily explains the lack of polarization at $\lambda 21$ cm where this equation yields $p \approx 0.2\%$ for $\sigma_{\text{RM}} = 200 \text{ rad m}^{-2}$. The Faraday depolarization is weaker at shorter wavelengths, with $p \approx 3\%$ at $\lambda 11$ cm and $p \approx 20\%$ at $\lambda = 6$ cm. However, the linear resolution of the observations of Thierbach et al. (2003) was $W = 110$ kpc at $\lambda 11.2$ cm and $W = 60$ kpc at $\lambda 6.2$ cm. Given that the thickness of the elongated polarized structures is of order $l_B = 25$ kpc, beam depolarization would further reduce the degree of polarization at least by a factor W/l_B to 0.5% at $\lambda 11.2$ cm and 8% at $\lambda 6$ cm. These estimates indicate that the polarization of cluster synchrotron halos should be weak but detectable at sufficiently high resolution and short wavelengths. In reality, each correlation cell may contain a few magnetic sheets with independent directions of magnetic field (cf. Fig. 5). Therefore, the effective number of magnetic sheets along the path length (and/or within the telescope beam) can be a factor 2–3 larger than adopted above and our values of the degree of polarization can be overestimated by a factor of two. Further polarization observations of cluster radio halos at short wavelengths can reveal magnetic structures suggested here.

Shear in the gas motions at a scale of a few hundred kiloparsecs, produced during major merger events, can make the random magnetic field locally anisotropic. The anisotropy can also be produced by differential rotation and/or inhomogeneous inflow in cluster cores. Anisotropic random magnetic field can produce significant polarization of the synchrotron emission, with the polarization vector orthogonal to the direction of the maximum r.m.s. field strength (Laing 1981; Sokoloff et al. 1998). This polarization can be observable if the shear regions are large enough as to avoid the cancellation of polarization along the line of sight or across the telescope beam.

Govoni et al. (2005) report detection of polarized emission from filamentary structures in the cluster A2255, of a size 200 kpc \times 500 kpc (see also Murgia et al. 2004), but the orientation of the polarization plane mostly disagrees with the above suggestions, unless the amount of foreground Faraday rotation is larger than that assumed by Govoni et al.

Another situation where significant polarization of synchrotron emission in the cluster environment can be ex-

pected are the wakes of subclusters and galaxies. Since individual lines of sight pass through one (or a few) wakes wherein the turbulent scale is comparable to the wake width, polarization due to the random magnetic field can be detectable.

6 DISCUSSION

There is growing direct and indirect evidence for the presence of random – and plausibly turbulent – motions in the intergalactic gas of galaxy clusters. We have identified several stages in their evolution, from a statistically quasi-steady motion during the epoch of major mergers, to the stage of decaying turbulence that follows, and to a state where turbulence is confined to the wakes of relatively small subclusters and individual galaxies. Typical parameters of the velocity and magnetic fields at various stages of the cluster evolution are summarized in Table 1: random velocities of $v_0 = 150\text{--}300\text{ km s}^{-1}$ can be maintained at various stages of the evolution, and their scale is expected to be $l_0 = 150\text{--}300\text{ kpc}$, with the exception of galactic wakes where it can be of the order of 10 kpc.

It is not quite clear whether or not the random motions in the intracluster gas can evolve into developed turbulence. This depends on the value of the Reynolds number, a measure of the relative strength of nonlinear hydrodynamic effects and, therefore, of the strength of the spectral energy cascade. If the flow remains laminar, the motions can decay faster after the end of the major mergers, and the wakes can have properties different from those discussed above. However, our numerical simulations suggest that the power-law decay establishes itself even for the Reynolds number as modest as $\text{Re} \simeq 100$.

The turbulent flow of magnetized gas can accelerate relativistic particles required to produce cluster radio halos (Tribble 1993b; Brunetti et al. 2004; Cassano & Brunetti 2005). Turbulent mixing in clusters has also been invoked in modeling the transport of heat (Cho et al. 2003; Kim & Narayan 2003; Voigt & Fabian 2004; Dennis & Chandran 2005), and metals (Rebusco et al. 2005). The dissipation of the turbulent energy can help to balance the cooling of cluster cores (Fujita, Matsumoto & Wada 2004; Rebusco et al. 2005). Clearly, turbulence in clusters seems to be useful to understand several diverse aspects of cluster physics.

Random motions during and immediately after the major merger epoch are plausibly volume-filling. However, random flows produced by the wakes can have area covering factor of order unity, but the volume filling factor of such wakes can be relatively small, $f_V \simeq 0.1$, leaving large quiescent regions between the wakes. Therefore, a typical line of sight passes through a turbulent region with an r.m.s. speed of a $200\text{--}300\text{ km s}^{-1}$, producing some observational signatures of developed turbulence, and yet there is enough space to accommodate well-ordered morphological features apparently unaffected by any random motions. For example, in the core of the Perseus cluster, where the density is higher (Churazov et al. 2004), with $n_e \geq 10^{-2}\text{ cm}^{-3}$ for $r \leq 100\text{ kpc}$, the mean free path is smaller $\lambda \leq 0.5\text{ kpc}$, and the wakes can have a potentially larger filling factors $f_V \leq 0.5$, for $\delta = 0.2$. Thus the presence of long $\text{H}\alpha$ filaments observed by Fabian et al. (2003, 2005) in the core of the Perseus cluster may

not be inconsistent with various evidence for random motions in this cluster core (Churazov et al. 2004; Rebusco et al. 2005). A possible signature of such spatially intermittent turbulence could be a specific shape of spectral lines, with a narrow core, produced in quiescent regions, accompanied by nonthermally broadened wings. It would be interesting to pursue this idea further in a more quantitative fashion.

In the presence of random motions, any pre-existing magnetic field will be rapidly destroyed owing to a reduction of its scale by the velocity shear. Even in a quiescent medium, any nonuniform magnetic would decay by driving motions whose kinetic energy can be efficiently converted into heat because the intracluster gas is expected to be rather viscous. Therefore, random magnetic fields confidently revealed in many clusters through their Faraday rotation must be constantly maintained even if the electrical conductivity of the intracluster gas is large.

However, the same random motions – either turbulent or not – will generate magnetic fields via the fluctuation dynamo action at all the stages of the cluster evolution. The field is amplified by random shear, which reduces its scale along the directions perpendicular to the shear layers. This makes the spatial distribution of the magnetic field intermittent. Numerical simulations give an impression of strong field regions being largely confined into magnetic sheets and ribbons (and, with lower probability, filaments) wherein its strength is similar to that given by energy equipartition with the overall kinetic energy density. Following Subramanian (1999), we argue that the volume filling factor of the magnetic structures within a turbulent cell (provided they are mostly sheets rather than filaments) is of order 0.1–0.2. Our numerical simulations confirm this picture, but add to it a weaker volume-filling magnetic background, so that the total magnetic energy density is about $1/5\text{--}1/3$ of the kinetic energy density of the random flow. The limited experience available with fluctuation dynamo models at large magnetic Prandtl number seems to indicate that magnetic fields can be closer to energy equipartition with turbulence in more realistic models.

The (random) Faraday rotation measures produced by such magnetic fields are in the 1σ range of $100\text{--}200\text{ rad m}^{-2}$ in agreement with observations. We note, however, that, according to our estimates, the scale of the magnetic field is $l_B = 20\text{--}40\text{ kpc}$, i.e., a factor of a few larger than what is usually assumed. The scale of the field is smaller, of order a kpc, for galactic wakes; it could also be smaller if there were other sources of stirring like radio galaxies. The maximum field strength in the magnetic structures is about $2\text{--}4\text{ }\mu\text{G}$, whereas its r.m.s. value within a turbulent cell is $1\text{--}2\text{ }\mu\text{G}$. Such r.m.s. field strengths are in better accord with those inferred from synchrotron intensity assuming equipartition between magnetic fields and cosmic rays, or with inverse Compton limits.

We predict that synchrotron emission from cluster radio halos similar to that in the Coma cluster can be significantly polarized at short wavelengths $\lambda = 3\text{--}5\text{ cm}$.

ACKNOWLEDGMENTS

We are grateful to R. Beck, A. Brandenburg, A. C. Fabian, L. Feretti and M. J. Rees for useful discussions. We appreci-

ate detailed comments of the referee, A. Schekochihin, which helped to improve the presentation. This work was supported by IUCAA, a joint grant program of the Indian National Science Academy and the Royal Society, and PPARC Grant PPA/G/S/2000/00528. AS and KS acknowledge the hospitality and partial financial support of the Isaac Newton Institute for Mathematical Sciences, Cambridge. AS is grateful to Carlo Barengi, Andrew Fletcher and Graeme Sarson who took over his teaching responsibilities during his stay in Cambridge.

REFERENCES

- Acreman D. M., Stevens I. R., Ponman T. J., Sakellou I., 2003, *MNRAS*, 341, 1333
- Bagchi J., Pislar V., Lima Neto G. B., 1998, *MNRAS*, 296, L23
- Balsara D., Livio M., O'Dea C. P., 1994, *ApJ*, 437, 83
- Batchelor G. K., 1950, *Proc. Roy. Soc. Lond.*, A201, 405
- Belyanin M., Sokoloff D., Shukurov A., 1993, *Geophys. Astrophys. Fluid Dyn.*, 68, 237
- Belyanin M. P., Sokoloff D. D., Shukurov A. M., 1994, *Russ. J. Math. Phys.*, 2, 149
- Biskamp D., 2003, *Magnetohydrodynamic Turbulence*, Cambridge Univ. Press, Cambridge
- Biskamp D., Müller W.-C., 1999, *Phys. Rev. Lett.*, 83, 2195
- Bondi H., 1952, *MNRAS*, 112, 195
- Brandenburg A., 2000, *Phil. Trans. Roy. Soc. Lond.*, A358, 759
- Brandenburg A., Subramanian K., 2005, *Phys. Rep.*, 417, 1
- Brunetti G., Blasi P., Cassano R., Gabici S., 2004, *MNRAS*, 350, 1174
- Brüggen M., Kaiser C. R., Churazov E., Enßlin T. A., 2002, *MNRAS*, 331, 545
- Burn B. J., 1966, *MNRAS*, 133, 67
- Carilli C. L., Taylor G. B., 2002, *ARAA*, 40, 319
- Cassano R., Brunetti G., 2005, *MNRAS*, 357, 1313
- Cattaneo F., 1999, *ApJ*, 515, L39
- Christensson M., Hindmarsh M., Brandenburg A., 2001, *Phys. Rev. E*, 64, 056405
- Cho, J., Lazarian, A., Honein, A., Knaepen, B., Kassinos, S., Moin, P., 2003, *ApJ*, 589, L77
- Churazov E., Forman W., Jones C., Sunyaev R., Böhringer H., 2004, *MNRAS*, 347, 29
- Clarke T. E., Kronberg P. P., Böhringer H., 2001, *ApJ*, 547, L111
- Clarke T. E., 2004, *JKAS*, 37, 1
- Colgate S. A., Li H., Pariev V., 2001, *Phys. Plasmas*, 8, 2425
- Colless M., Dunn A. M., 1996, *ApJ*, 458, 435
- Christensson M., Hindmarsh M., Brandenburg A., 2001, *Phys. Rev. E* 64, 056405
- De Young, D. S., 1992, *ApJ*, 386, 464
- Dennis, T. J., Chandran, B. D. G., 2005, *ApJ*, 622, 205
- Dolag K., Bartelmann M., Lesch H., 1999, *A&A*, 348, 351
- Dolag K., Bartelmann M., Lesch H., 2002, *A&A*, 387, 383
- Eilek, J. A., Owen, F. N., 2002, *ApJ*, 567, 202
- Enßlin T. A., 2003, *A&A*, 399, 409
- Enßlin T. A., Heinz S., 2002, *A&A*, 384, L27
- Enßlin T. A., Vogt, C., 2003, *A&A*, 401, 835
- Enßlin, T. A., Vogt, C., Clarke, T. E., Taylor, G. B., 2003, 597, 870
- Fabian A. C., Daines S. J., 1991, *MNRAS*, 252, 17P
- Fabian A. C., Sandres J. S., Crawford C. S., Conselice C. J., Gallagher J. S., Wyse R. F. G., 2003, *MNRAS*, 344, L48
- Fabian A. C., Reynolds C. S., Taylor G. B., Dunn R. J. H., 2005, *MNRAS* (submitted); *astro-ph/0501222*
- Frisch U., 1995, *Turbulence. The Legacy of A. N. Kolmogorov*. Cambridge Univ. Press, Cambridge
- Fujita, Y., Matsumoto, T., Wada, K., 2004, *ApJ*, 612, L9
- Furlanetto S. R., Loeb A., 2001, *ApJ*, 556, 619
- Goldman I., Rephaeli Y., 1991, *ApJ*, 344, 350
- Goldshmidt O., Rephaeli Y., 1994, *ApJ*, 431, 586
- Govoni F., Feretti L., 2004, *Int. J. Mod. Phys. D*, 13, 1549
- Govoni F., Murgia M., Feretti L., Giovannini G., Dallacasa D., Taylor G. B., 2005, *A&A*, 430, L5
- Haugen N. E. L., Brandenburg A., Dobler W., 2003, *ApJ*, 597, L141
- Haugen N. E. L., Brandenburg A., Dobler W., 2004, *Phys. Rev. E*, 70, 016308
- Heinz S., Churazov E., Forman W., Jones C., Briel U. G., 2003, *MNRAS*, 346, 13
- Inogamov N. A., Sunyaev R. A., 2003, *Astron. Lett.*, 29, 791
- Jaffe W., 1980, *ApJ*, 241, 925
- Johnston-Hollitt, M., Ekers, R. D., 2004, *astro-ph/0411045*.
- Kazantsev A. P., 1967, *JETP*, 53, 1806
- Kim E.-J., 1999, *Phys. Lett. A*, 259, 232
- Kim, W.-T., Narayan, R., 2003, *ApJ*, 596, 139
- Kronberg P. P., 1994, *Rep. Progr. Phys.*, 57, 325
- Kulsrud R. M., Cen R., Ostriker J. P., Ryu D., 1997, *ApJ*, 480, 481
- Lacey C., Cole S., 1993, *MNRAS* 262, 627
- Laing R. A., 1981, *ApJ*, 248, 87
- Landau L. D., Lifshitz E. M., 1975, *Fluid Mechanics*, Pergamon Press, Oxford
- Maron, J., Cowley, S., McWilliams, J., 2004, *ApJ*, 603, 569
- Medina-Tanco G., Enßlin T. A., 2001, *Astroparticle Phys.*, 16, 47
- Meneguzzi M, Frisch U, Pouquet A., 1981. *Phys. Rev. Lett.*, 47, 1060
- Monin A. S., Yaglom A. M., 1975, *Statistical Fluid Mechanics*, Vol. 2, MIT Press, Cambridge
- Motl, P. M., Burns, J. O., Loken, C., Norman, M. L., Bryan, G., 2004, *ApJ*, 606, 635
- Murgia M., Govoni F., Feretti L., Giovannini G., Dallacasa D., Fantì R., Taylor G. B., Dolag K., 2004, *A&A*, 424, 429
- Norman M. L., Bryan G. L., 1999, in Röser H.-J., Meisenheimer K., eds, *The Radio Galaxy Messier 87*, Lecture Notes in Physics 530, Springer-Verlag, p. 106
- Nulsen P. J. E., 1982, *MNRAS*, 198, 1007
- Olesen P., 1997, *Phys. Lett.*, B398, 321
- Padmanabhan, T., 1993, *Structure Formation in the Universe*, Cambridge Univ. Press, Cambridge
- Padmanabhan T., Subramanian K., 1992, *Bull. Astron. Soc. India*, 20, 1
- Peebles P. J. E., 1980, *Large-Scale Structure of the Universe*, Princeton Univ. Press
- Portnoy D., Pistinner S., Shaviv G., 1993, *ApJS*, 86, 95
- Rebusco P., Churazov E., Böhringer H., Forman W., 2005, *MNRAS* (in press); *astro-ph/0501141*
- Rees M. J., 1994, in Lynden-Bell D., ed., *Cosmical Magnetism*, NATO Adv. Sci. Inst. (ASI) Series C, Vol. 422, p. 155
- Reynolds, C. S., Heinz, S., Begelman, M. C., 2002, *MNRAS*, 332, 271
- Ricker P. M., Sarazin C. L., 2001, *ApJ*, 561, 621
- Roettiger K., Stone J. M., Burns J. O., 1999a, *ApJ*, 518, 594
- Roettiger K., Burns J. O., Stone, J. M., 1999b, *ApJ*, 518, 603
- Roland J., 1981, *A&A*, 93, 407
- Rudnick, L., Blundell, K. M., 2003, *ApJ*, 588, 143
- Ruzmaikin A., Sokoloff D., Shukurov A., 1989, *MNRAS*, 241, 1
- Sakellou I., Acreman D. M., Hardcastle M. J., Merrifield M. R., Ponman T. J., Stevens, I. R., 2005, *MNRAS*, 360, 1069
- Sanderson A. J. R., Ponman, T. J., 2003, *MNRAS*, 345, 1241
- Sarazin C. L., 1988, *X-Ray Emission from Clusters of Galaxies*, Cambridge University Press
- Schekochihin A. A., Cowley S. C., Taylor S. F., Maron J. L., McWilliams J. C., 2004, *ApJ*, 612, 276
- Schekochihin A. A., Cowley S. C., Kulsrud R. M., Hammett G. W., Sharma P., 2005a, in *The Magnetized Plasma*

in Galaxy Evolution, Eds K. T. Chyży, R.-J. Dettmar, K. Otmianowska-Mazur, M. Soida, Jagiellonian Univ., Kraków; astro-ph/0411781

Schekochihin A. A., Cowley S. C., Kulsrud R. M., Hammett G. W., Sharma P., 2005b, *ApJ*, 629, 139

Schuecker P., Finoguenov A., Miniati F., Böhringer H., Briel U. G., 2004, *A&A*, 426, 387

Skrbek L., Stalp S. R., 2000, *Phys. Fluids*, 12, 1997

Sokoloff D. D., Bykov A. A., Shukurov A., Berkhuijsen E. M., Beck R., Poezd A. D., 1998, *MNRAS*, 299, 189; Erratum: 1999, *MNRAS*, 303, 207

Subramanian K., 1997, astro-ph/9708216

Subramanian K., 1999, *Phys. Rev. Lett.*, 83, 2957

Subramanian K., 2003, *Phys. Rev. Lett.*, 90, 245003

Sun M., Vikhlinin A., Forman W. Jones C., Murray S. S., 2005, *ApJ*, 619, 169

Sunyaev R. A., Norman M. L., Bryan G. L., 2003, *Astron. Lett.*, 29, 783

Takeda H., Nulsen P. E. J., Fabian A. C., 1984, *MNRAS*, 208, 261

Takizawa M., 2005, *ApJ* (in press); astro-ph/0505274

Thierbach M., Klein U., Wielebinski R., 2003, *A&A*, 397, 53

Tomboulides A. G., Orszag S. A., 2000, *JFM*, 416, 73

Toniazzo T., Schindler S., 2001, *MNRAS*, 325, 509

Touil H., Bertoglio J.-P., Shao L., 2002, *J. Turbulence*, 3, 049

Tribble P., 1993a, *MNRAS*, 263, 31

Tribble P. C., 1993b, in *Cosmical Magnetism. Contributed Papers in Honour of Prof. L. Mestel* (D. Lynden-Bell, ed.). Cambridge, Inst. Astron, p. 140

Vogt C., Enßlin T. A., 2003, *A&A*, 412, 373

Vogt C., Enßlin T. A., 2005, *A&A*, 434, 67

Voigt, L. M., Fabian, A. C., 2004, *MNRAS*, 347, 1130

Widrow L. M., 2002, *Rev. Mod. Phys.*, 74, 775

Zeldovich Ya. B., Ruzmaikin A. A., Sokoloff D. D., 1990, *The Almighty Chance*, World Scientific, Singapore

APPENDIX A: SEED MAGNETIC FIELDS IN GALAXY CLUSTERS

There is a number of sources of seed magnetic fields in galaxy clusters. It is well known that the intracluster medium (ICM) has high metallicity which must have been produced in stars in galaxies and subsequently ejected into the galactic interstellar medium (ISM) and then into the ICM. Since the ISM is likely to be magnetized with fields of order a few μG , this would lead to a seed field in the ICM. One can roughly estimate the seed field resulting from stripping the galactic gas, by using magnetic flux conservation under spherically symmetric expansion; that is $B_{\text{seed}} \simeq (\rho_{\text{ICM}}/\rho_{\text{ISM}})^{2/3} B_{\text{gal}}$. For $B_{\text{gal}} \simeq 3 \mu\text{G}$, and $\rho_{\text{ICM}}/\rho_{\text{ISM}} \simeq 10^{-2}-10^{-3}$, one gets $B_{\text{seed}} \simeq 0.1-0.03 \mu\text{G}$. One may get even larger seed fields if there is a substantial number of active galaxies with magnetized outflows: if about 10^3 galaxies have mass outflow with $\dot{M} \simeq 0.1 M_{\odot} \text{ yr}^{-1}$ lasting for 1 Gyr, with a Poynting flux about 10% of the material flux, and the field gets mixed into the cluster gas over a Mpc sized region, $B_{\text{seed}} \simeq 0.3 \mu\text{G}$ would result (Brandenburg 2000). This estimate, however, assumes that all the intracluster gas has been processed through the outflows, which may be an exaggeration.

Another source of seed fields is likely to be the outflows from earlier generation of active galaxies (radio galaxies and quasars) (Rees 1994; Goldshmidt & Rephaeli 1994; Medina-Tanco & Enßlin 2001; Furlanetto & Loeb 2001; Colgate, Li & Pariev 2001). Such outflows can produce magnetized plasma

bubbles in some fraction of the intergalactic volume (typically of order 10% – Furlanetto & Loeb 2001) which, when incorporated into the ICM, would seed the general cluster gas with magnetic fields. If one assumes that the cluster gas is 10^3 times denser than the intergalactic medium and blindly uses the enhancement of the bubble field due to compressions during cluster formation, one can get fields as large as $0.1-1 \mu\text{G}$ in the ICM (Furlanetto & Loeb 2001). However this is to ignore the issue of how the field in the magnetized bubble, especially if it is predominantly relativistic plasma from a radio galaxy, mixes with the unmagnetized and predominantly thermal gas during cluster formation, and the resulting effects on both the field strength and coherence scale (see Enßlin 2003 for the related problem of the escape of cosmic rays out of radio cocoons). It is likely that, while AGNs and galaxies provide a potentially strong seed magnetic field, there would still be a need for their subsequent amplification and maintenance against turbulent decay.

Altogether, we adopt $B_{\text{seed}} = 10^{-7} \text{ G}$ as a plausible estimate of the seed magnetic field in the intracluster gas.

APPENDIX B: THE CORRELATION FUNCTION OF THE FARADAY ROTATION MEASURE

In order to calculate the autocorrelation function of the Faraday rotation measure, defined in Eq. (26), we introduce coordinates (x, y, z) with the z -axis directed towards the observer, and those in the plane of the sky, $\mathbf{X} = (X, Y)$. We assume the magnetic field to be an isotropic, homogeneous, random field with zero mean value. Then its equal-time, two-point correlation tensor has the form $\langle B_i(\mathbf{x}, t) B_j(\mathbf{y}, t) \rangle = M_{ij}(r, t)$, where

$$M_{ij} = \left(\delta_{ij} - \frac{r_i r_j}{r^2} \right) M_N(r, t) + \frac{r_i r_j}{r^2} M_L(r, t).$$

Here $\langle \dots \rangle$ denotes the ensemble average, $r = |\mathbf{x} - \mathbf{y}|$, and $r_i = x_i - y_i$ (see Section 34 of Landau & Lifshitz 1975; Monin & Yaglom 1975). The functions $M_L(r, t)$ and $M_N(r, t)$ are known as the longitudinal and transverse correlation function of the magnetic field, respectively. Since $\nabla \cdot \mathbf{B} = 0$,

$$M_N = \frac{1}{2r} \frac{\partial}{\partial r} (r^2 M_L).$$

We also assume for simplicity that the electron density is uncorrelated with the magnetic field and also constant over the field correlation length. This is consistent with the fact that random gas motions in galaxy clusters are quite subsonic. The correlation function of RM is then

$$\begin{aligned} C(R) &= \langle \text{RM}(\mathbf{X}_1) \text{RM}(\mathbf{X}_2) \rangle \\ &= K^2 n_e^2 \int_0^L \int_0^L \langle B_z(\mathbf{X}_1, z_1) B_z(\mathbf{X}_2, z_2) \rangle dz_1 dz_2 \\ &= K^2 n_e^2 L \int_{-L}^L M_{zz}(R, \zeta) d\zeta \\ &= K^2 n_e^2 L \int_{-L}^L \left(M_L \frac{R^2}{R^2 + \zeta^2} + M_N \frac{\zeta^2}{R^2 + \zeta^2} \right) d\zeta \\ &= K^2 n_e^2 L \int_{-L}^L \left(M_L + \frac{\zeta^2}{2r} \frac{dM_L}{dr} \right) d\zeta. \end{aligned} \quad (\text{B1})$$

Here we have assumed that L is much greater than the correlation length of the magnetic field, $\zeta = z_1 - z_2$, $R = |\mathbf{X}_1 - \mathbf{X}_2|$ and $r^2 = R^2 + \zeta^2$.

For the sake of illustration, consider the longitudinal correlation function of the form

$$M_L = \frac{1}{3} \langle B^2 \rangle \exp\left(-\frac{r^2}{2l_B^2}\right),$$

which corresponds to the one-dimensional magnetic spectrum of the form $M_k \propto k^4 \exp(-k^2 l_B^2/2)$ (Monin & Yaglom 1975). We note that M_k attains maximum at a wavenumber $k_m = 2/l_B$, (or a scale $2\pi/k_m = \pi l_B$), whereas the longitudinal correlation scale is given by $l_L = [M_L(0)]^{-1} \int_0^\infty M_L(r) dr = l_B \sqrt{\pi/2}$.

Straightforward calculation then yields

$$C(R) = \frac{\sqrt{2}}{3} c K^2 n_e^2 \langle B^2 \rangle L l_B \exp\left(-\frac{R^2}{2l_B^2}\right), \quad (\text{B2})$$

where

$$c = \int_{-L/(\sqrt{2}l_B)}^{L/(\sqrt{2}l_B)} (1 - s^2) \exp(-s^2/2) ds \approx 0.88,$$

with the numerical value obtained for $L/(\sqrt{2}l_B) \gg 1$.

The r.m.s. value of RM can be obtained from Eq. (B1) or (B2) at $R = 0$:

$$\begin{aligned} \sigma_{\text{RM}}^2 &= K^2 n_e^2 L \int_{-L}^L M_N(R, z)|_{R=0} d\zeta \\ &= \frac{\sqrt{2}}{3} c K^2 n_e^2 \langle B^2 \rangle L l_B, \end{aligned} \quad (\text{B3})$$

which is similar to Eqs (27) and (28).